Supplementary Information for

A unifying model for the accretion of chondrules and matrix

Elishevah van Kooten, Frédéric Moynier and Arnaud Agranier

Elishevah van Kooten.
E-mail: vankooten@ipgp.fr

This PDF file includes:

Supplementary text
Figs. S1 to S20
Table S1
References for SI reference citations

Supporting Information Text

Materials

Leoville. Leoville is considered an accretionary breccia and is among the least altered reduced CV chondrites and experienced only mild thermal metamorphism and compaction. We note that even though Leoville is relatively unaltered, element mobilization from matrix to chondrules has been reported for moderate volatiles such as Na and S in ordinary chondrites with similar alteration degrees (1). Leoville is a find and regions of the meteorite suffered cracking and subsequent terrestrial weathering, resulting in metal-loss and vein filling. For this study, we have chosen a metal-rich area, with a low degree of weathering, although Fe-rich veins occur throughout the section. Areas directly surrounding large veins were avoided. The chondrules of Leoville are densely packed and limited intra-chondrule matrix is present between the fine-grained dust rims of the chondrules. The intra-chondrule matrix is distinguishable from the dust rims by being more coarse-grained (Fig. S1). Porphyritic olivine (PO) and porphyritic olivine pyroxene (POP) chondrules represent the majority of chondrules in Leoville and other chondrules have barred textures. Most chondrules have either sulfide-rich fine-grained igneous rims (reflecting multiple melting events) or low-Ca pyroxene rich rims (reflecting a single melt event). In addition, a fair amount of chondrules has a metal/sulfide rim surrounding the primary core of the chondrule. We have selected two PO chondrules (A-Ch2 and B-Ch1) and one POP chondrule (B-Ch6) from both sides of a 2×2 cm thick section of Leoville. The PO chondrules are 2-3 mm in diameter, whereas the PO chondrule is ∼1 mm in diameter. The PO chondrules contain cores with euhedral/subhedral forsteritic olivine phenocrysts (∼100 µm), Ca-Al rich mesostasis and FeNi metal, which gradually transitions towards the rim with smaller forsteritic olivine and low-Ca pyroxene phenocrysts (<50 µm) as well as more troilite relative to metal. The boundary between chondrule and dust rim is irregular and the dust rims are ∼200 µm thick. The PO chondrule has a very round shape and is very rich in mesostasis relative to other chondrules in this section. It contains a single forsterite phenocryst and otherwise euhedral low-Ca pyroxene phenocrysts surrounded by zonation of Ca-rich pyroxene. The mesostasis appears glassy rather than crystalline. The entire chondrule is surrounded by a metal and pyroxene rim, where the pyroxene seems partially substituted by Ca-rich pyroxene. The surrounding dust rim is in direct contact with the metal-rich rim and is approximately 200 µm thick.

Vigarano. Vigarano is the prototype of the CV chondrites and is a reduced CV chondrite, similar to Leoville. Vigarano is an observed fall and contains regions with low alteration degrees comparable to Leoville (i.e., petrological type 3.1) as well as more altered regions (i.e., <3.4). We have selected chondrules from the least altered regions: two barred chondrules (e.g., Ch3 and Ch13, ∼2 mm in diameter, Fig. S2), with Ch13 containing a core with a lath-shaped forsteritic olivine and a glassy Ca-Al-rich mesostasis and a thick (∼300 µm) olivine- and metal-rich chondrule rim. Ch3 is perfectly rounded and consists of a single core texture with lath-shaped forsteritic olivine and a glassy Ca-Al-rich mesostasis. Ch13 is surrounded by a fine-grained layered dust rim, being more Mg-poor and sulfide-rich towards the chondrule. Both the core and the rim materials were sampled during LA-ICPMS analyses. Ch3 does not contain a distinct dust rim, and appears more like a separate clast within the section. We sampled another chondrule with a PO texture (Ch5), consisting of a primary and a secondary core, separated by a metal rim. The primary core has a higher forsterite/mesostasis ratio than the secondary core. Furthermore, Ch5 is bounded by a thick olivine-rich rim (∼200 µm). The chondrule is surrounded by a fairly uniform dust rim of approximately ∼200 µm. Finally, we sampled only the dust rim of Ch6 by LA-ICPMS, since this rim is uniquely thick and allows for sampling, uncontaminated by chondrule material.

Allende. Allende is an oxidized CV chondrite, which is an observed fall and represents a more severely thermally altered chondrite (i.e., CV>3.6) than Leoville and Vigarano. The relatively high degree of alteration can be observed throughout the thick section: the matrix is more coarse-grained and the chondrules show significant chemical alteration at their boundaries (Fig. S3). Fine-grained dust rims are not observed and matrix samples were taken from the direct vicinity of the chondrule-matrix boundaries. We have selected one barred chondrule (Ch1) and two PO chondrules (Ch2 and Ch4) with diameters of 1-2 mm. Ch1 consists of lath-shaped forsteritic olivine and a mesostasis that is partially recrystallized to Ca-rich pyroxene and anorthitic feldspar. The boundaries of the chondrule are chemically altered towards a more Fe-rich composition, whereas the chondrule core is relatively Fe-poor. The suggestion of a dust rim is present, by absence of coarse pyroxene and sulfides in the matrix. The PO chondrule Ch2 consists of a core with large forsterite phenocrysts (<300 µm) and a low abundance of crystallized mesostasis. The chondrule rim contains relatively more mesostasis and finer olivine phenocrysts (<50 µm). This rim also contains large rounded sulfides, which appear to be alteration products of primary metal. The boundary of the rim is chemically altered to more Fe-rich, Mg-poor compositions, towards a similar composition as the surrounding matrix. Ch4 is perfectly rounded and consists of large forsterite phenocrysts, increasing in size towards the chondrule boundary (100-300 µm), in a recrystallized mesostasis. Similar to Ch1 and Ch2, the chondrule boundary is chemically altered.

Maribo. Maribo is an observed fall and one of the most unaltered CM chondrites in our meteorite collection (petrological type = CM>2.8), similar to Paris (2–4). The thick section (0.5 × 0.5 cm) of Maribo consists of homogeneously distributed tochilinite-cronstedtite intergrowths (TCIs), porphyritic chondrules and small CAIs surrounded by dust rims, which constitute all matrix in the chondrite. We do not consider the TCIs as part of the matrix, since they may have formed before accretion of the CM parent body and have dust rims themselves. Large metal grains are absent in Maribo, but small metal nuggets are found in the matrix (4). Chondrules are typically small in size (on average ∼200-300 µm) and mostly consist of single rimless cores with a PO or POP texture. We have selected two 'average' chondrules (Ch1 and Ch4, 300-400 µm) and one larger than average chondrule (Ch8, 500 × 1000 µm), all with similar POP textures (Fig. S4). The matrix mineralogy and composition of

Elishevah van Kooten, Frédéric Moynier and Arnaud Agranier

this section have been recently reported by (4). Although the CM chondrules are typically an order of magnitude smaller than CV chondrules, their fine-grained dust rims are similar in thickness (on average 200 μm thick).

Cold Bokkeveld. Cold Bokkeveld represents one of the most altered CM2 chondrites (petrological type = CM2.2) and is chosen as the 'altered version' of the CM chondrites above more typical CM2 chondrites such as Murchison and Mighei (CM2.5) to emphasize the potential compositional variations produced during aqueous alteration. Cold Bokkeveld is an observed fall. Chondrules in Cold Bokkeveld are similar to those observed in Maribo (e.g., size, texture), but are more altered: sampled Ch1, Ch2 and Ch8 chondrules show crystallized Ca-rich pyroxene and feldspar in the mesostasis as well as the presence of sulfides within the chondrule (Fig. S5). The dust rims of Cold Bokkeveld chondrules are on average 200 μm thick, similar to Maribo, but contain a larger abundance of Fe sulfides, sometimes in layered structures (Ch1 and Ch2). In addition to the three chondrules, we selected Ch7 for matrix analyses by LA-ICPMS, since the dust rim was uniquely large in size to avoid contamination from underlying chondrules.

NWA801. NWA801 is the only CR2 chondrite selected for this study, since no CR3 chondrites were available to us at the time. It is clear, however, that NWA801 underwent negligible thermal metamorphism (5) and that CR2 chondrites in general experienced only mild aqueous alteration (6, 7). CR2 chondrites have been classified according to their degree of alteration (8) in a similar way as CM chondrites (9). The chondrules in NWA801 reflect limited evidence of aqueous alteration, containing abundant FeNi metal blebs and a relatively unaltered mesostasis. In addition, the dust rims are interspersed with the metal rims irregularly surrounding the chondrules and are sulfur-rich in most cases (Fig. S6) and generally have a low MgO abundance (average of 15.6 wt.%, Fig. S7, suggesting that these dust rims were not significantly altered (1, 8, 10). The metal in NWA801 is altered to some extent, but the oxidized rinds around the metal grains may be indicative of terrestrial weathering rather than aqueous alteration. Other evidence for terrestrial weathering is in the form of cracks and Fe-rich veins running through the thick section. These veins and their direct surroundings were avoided during analyses. The chondrules in NWA801 are typically PO and POP type and contain abundant metal within the chondrule as well as in the chondrule rims. The intra-chondrule matrix, on the other hand, is rich in Fe sulfides rather than metal (Fig. S6). Ch1 and Ch2 are 1-2 mm in diameter and consist of euhedral/subhedral forsterite phenocrysts ($\sim$100-300 μm) in a glassy mesostasis. Ch2 contains abundant metal within the chondrule. The dust rim of Ch1 is sulfide-poor, whereas the rim in Ch2 is sulfide-rich. The thickness of the dust rims is approximately 100-200 μm. Ch3 is a POP chondrule (<1 mm), with abundant low-Ca pyroxene interspersed between the subhedral/euhedral Fe-poor olivine. The dust rim surrounding Ch3 is sulfide-poor and metal-rich, similar to the dust-rim around Ch1.

Methods

SEM. Before LA-ICPMS analyses, SEM/EDS analyses were carried out to characterize the petrology and petrological context of the samples and to obtain major element compositions of the regions of interest. LA-ICPMS analyses require the a priori knowledge of a major element concentration such as Mg or Ca, to use for internal calibration. Together with external calibration using known reference standards, this provides high precision analyses of major, minor and trace elements (see LA-ICPMS Methods in SI Appendix). Since the aim was to measure bulk compositions of chondrules and their rims, we have first made elemental maps of the chondrules using SEM/EDS, after which we quantified the major element concentrations using a standardless procedure, also known as a semi-quantitative analyses. The advantage of this method is to rapidly define the bulk compositions of large areas, such as chondrules, even after LA-ICPMS analyses. Usually, high precision electron microprobe (EMP) analyses are done on smaller areas before LA-ICPMS analyses, but the small EMP beam size ($\sim$10 μm) does not reflect the bulk of the chondrule well (0.2 - 2 mm). Moreover, the generation of EMP elemental maps is very time consuming. Nevertheless, standardless analyses by SEM/EDS can potentially introduce large errors to the analyses if not handled correctly: (1) standardless analyses require that the calculated concentrations must be internally normalized to a sum of unit, which is not always realistic; (2) the geometry of the sample can produce errors if the surface is too rough (also in analyses using standards); (3) mis-identification of elements in an EDS spectrum can lead too erroneous results. Minor element analyses can, thus, lead to 2SD errors of 30-50% (11). Nevertheless, for our purpose of defining major element Mg, Fe and Si concentrations in the regions of interest, we show here that we can obtain reliable results within a few wt.% error, which is sufficient for the purpose of LA-ICPMS calibration. We have compared matrix and chondrule compositions from standardless SEM/EDS with our laser ablation data, as well as with independently obtained literature data by LA-ICPMS, wet analyses and Instrumental Neutron Activation Analysis (INAA). These comparisons show that our results are accurate within a few weight percent. For example, the Fe, Mg and Si concentrations of Maribo matrix are identical to matrix from Paris (Fig. S7, 3). Moreover, the average LA-ICPMS Fe concentrations obtained by normalization to Mg are very similar to average Fe concentrations from SEM/EDS quantification for Maribo and NWA801 matrix and CM, CV and CR chondrule compositions. The CV chondrite matrix from Leoville, Vigarano and Allende has higher Fe concentrations from SEM/EDS analyses than from LA-ICPMS, wet analyses and INAA, but overall shows the same trend as SEM data: Leoville matrix has a higher Fe abundance relative to Maribo and Allende has lower Fe/Mg ratios than Leoville, plotting near the CI ratio. This discrepancy between SEM data and other techniques could be caused by 1) Contamination of the matrix from underlying chondrules during laser ablation or micro-drilling, 2) An analytical artifact during SEM/EDS analyses. Phases that contain Fe, when measured by EMP or SEM, are denser than surrounding phases, resulting in an underestimation of the Fe concentration (12–14). Since the Fe concentration from CV matrix SEM data is higher than by other techniques and Maribo matrix by SEM is in full agreement

with these techniques, we suggest that the lower CV matrix concentrations are the result of chondrule contamination. This contamination amounts to <15 %, when mass balancing chondrule and matrix average data.

LA-ICPMS. LA-ICPMS measurements were performed at the Institut Universitaire Européen de la Mer (Brest) and ablation was conducted using a 193 nm Compex Pro 102 Coherent Laser Ablation System, for which the energy output was 15 J/cm^2 and the laser frequency was 10 Hz. Following the size of the chondrules and the dust rims, we have applied spot sizes of 90-160 µm and 60-120 µm, respectively. Helium gas was flushed into the ablation cell, holding the thick sections, thereby minimizing aerosol deposition around the ablation pit and improving transport efficiency. Laser-induced aerosol particles were carried by helium and then mixed with argon before entering the plasma. The laser ablation system was coupled to an Element XR high resolution mass spectrometer, which has the advantage of a large linear dynamic detection range, highly suitable for simultaneous major element and ultra-trace element analyses. The 33 analyzed isotopes are presented in Table S1 and are sorted according to their 50% condensation temperature (15). Each measurement consisted of 50 cycles with a total analyses time of 180 seconds. The first ten cycles were used for background measurement of the gas blank, after which the laser firing time lasted 40 cycles. Between measurements, approximately 2 minutes were taken to flush the ablation cell and reduce memory effects. Per chondrule and dust rim, typically three spots were ablated. For some CV chondrules, a distinction was made between chondrule core and igneous rim. Data corrections were carried out using GLITTER software to correct for deadtime (24 ns) and subsequent manual data reduction was done to subtract the background and normalize to Mg for the last 30 cycles. Mg was chosen as the internal calibration element, since SEM/EDS data obtained more reliable Mg concentrations over Ca, the samples often containing <1 wt.% Ca. From the normalized data, outliers were manually removed and the resulting relative standard deviation (2σ) was typically <10% for major and minor elements and <20% for trace elements in the samples, and was generally better for the chondrules than the matrix. Most of this uncertainty stemmed from heterogeneities within the ablated spot. The Rb and Cs concentrations were often below detection limits in the chondrules and sometimes also in the matrix. These data were removed from consideration. At the beginning and end of each analyses session, terrestrial standard glasses BCR2, BIR1 and BHVO-2 were measured multiple times along with synthetic glasses NIST612 and NIST610, which were doped with trace elements. Since the overall composition of our samples was much closer to that of terrestrial standards (e.g., trace element concentrations of NIST standards are generally orders of magnitude higher), we chose to use only the natural terrestrial standards for external calibration. This was done by correcting our unknown samples to the regression slope obtained by plotting the measured elemental concentrations of the standards against known concentrations from literature.

Results and discussion

The weathering grade of chondrites. As discussed in the main text, certain peaks of highly mobile elements (e.g., U, Sr, Ba, Eu) are observed in the volatility patterns of Maribo chondrules and matrix. Moreover, similar, but less pronounced peaks are also observed in CV chondrules and matrix, causing both chondritic components to more or less track each other (Fig. S12). This observation could indicate several things: 1) these peaks are primary features that suggest an elemental fractionation of chondrule and matrix precursors before chondrule formation, 2) the sampled matrix was contaminated by chondrules and 3) these peaks are the result of terrestrial weathering and/or early onset of secondary alteration on the chondrite parent body. We explain below why we prefer the third interpretation. First, we have trouble envisioning how such a pattern would be produced by fractionating the precursors of chondrules and matrix before the chondrules were formed, as there is no correlation to volatility and more with the mobility of elements in an aqueous state. Second, although the CV matrix patterns could indicate some contamination of chondrules, this is less likely for the CM matrix, since the chondrule and matrix patterns are nearly identical. The most likely interpretation is that the peaks and valleys observed in both chondrules and matrix are the product of terrestrial weathering or leaching during the onset of secondary alteration, since it seems to affect mainly the highly mobile elements such as U, Sr, Ba, Rb and Cs (16). A more thorough assessment of weathering grade and mobility of elements would be necessary to determine if this interpretation is correct, but is difficult to do with the data at hand. For example, bulk compositions of CM chondrites Nogoya, Murchison and Cold Bokkeveld show similar peaks as Maribo (17), but their weathering grade is not determined. Moreover, the weathering grade of chondrites is established through different techniques. Until the 90's, the weathering grade was determined from the relative rustiness of hand specimens (grades A, B, C) and from then on a scale was set up that looked more carefully at the changes in mineralogy of polished sections (W0-W6; 18). As a result, the weathering grade of CM chondrites is determined by different methods or not determined at all (17). Furthermore, the nature and extent of the terrestrial weathering is dependent on the climate in which the meteorite has resided and the duration of weathering. For example, mobilization of elements is different for hot and cold deserts. Maribo, although being an observed fall, was recovered from a field in Denmark after being subjected to two months of freezing and rain showers, and because of its high porosity was easily weathered, which may explain its high Na content (2). This type of weathering is not easily comparable with meteorites that have been subjected to different climates. We therefore submit that the conditions in which Maribo was found, are likely unique to the chondrite, but that the peaks in U, Sr, Ba, Rb, Cs, relative to CI composition, are most likely caused by terrestrial alteration.

Model-dependent deductions of CM matrix composition. We have shown using volatility dependent element abundance patterns that the Maribo matrix does not record volatile loss. In contrast, Cold Bokkeveld, a more heavily altered CM chondrite reflects increased volatile depletion and transfer of mobile elements (e.g., Sr, Ba, U) from the matrix. A CI-like matrix for the most unaltered CM chondrite Maribo, is in agreement with matrix data from Paris (another relatively unaltered CM chondrite,

Elishevah van Kooten, Frédéric Moynier and Arnaud Agranier

(3)) and presolar grain abundances from Murchison and Murray (19), which all point to a CI-like matrix composition. In addition, there is indirect and model-dependent evidence that CM chondrites have accreted a CI-like matrix. For many isotope and element systems, CM chondrites plot between CI and CO chondrites, suggesting that CM chondrites accreted CO-like chondrules and CI-like matrix. For example, in O (three isotope plot, 20, 21), Ca versus Ti (stable isotopes, 22, 23), O versus Cr (24) isotope space CM chondrites fall on a mixing line between CO and CI chondrites. Although these data point towards a CI-like composition of the CM matrix, in agreement with our data, we stress that such models do not take into consideration the fact that CM chondrites do not only consist of chondrules and matrix, but also contain tochilinite-cronstedtite intergrowths (TCIs, which probably not part of the matrix), CAIs and metal. Hence, only direct measurements of matrix and chondrules can provide firm model-independent evidence of the relationship between these chrondritic components. The bulk of chondrites can not be used to infer relationships between chondrules and matrix, because chondrites are not binary systems.

REE spidergrams. The rare earth element patterns are normalized against CI abundances (15). For Leoville and Vigarano CV chondrites, we observe overall flat REE patterns, with on average 3×CI composition and ranging between 1-4×CI for individual chondrules. All chondrule patterns are either completely flat or show a minor enrichment or depletion in Eu, resulting in an overall slight depletion for average CV chondrules. This anomaly is suggested to be the result of a small contribution from refractory inclusions to the chondrule precursor (25). Chondrule B-Ch6 from Leoville is very distinct and shows a depletion trend towards HREE elements, with La having >10×CI and Lu CI-like abundances (Fig. S10A). Within this trend, we observe a positive anomaly for Yb. This chondrule also has a distinct Al-rich petrology with abundant mesostasis. Al-rich chondrule REE patterns are associated with those of refractory inclusions (25), also explained the general enrichment of refractory elements in B-Ch6 (Fig. 2, main text). Our results are in agreement with previous chondrule REE analyses of Leoville (25). The REE patterns of chondrule igneous rims are flat and closely resemble those of the chondrule cores, albeit being more depleted on average. The average REE pattern of CV matrix is very similar to that of the chondrules, albeit with a strong positive Eu anomaly (likely attributed to terrestrial weathering, 25) and CI-like abundances. Despite the CI-like REE abundances of the matrix and the interpretation of the positive Eu anomaly being a secondary feature, (25) view the EU anomalies as evidence for complementarity. In our view, the matrix REE composition of relatively unaltered CV chondrites can only be interpreted as being unfractionated and CI-like, with perhaps a minor contamination from refractory inclusions that accreted together with the matrix. This contamination is estimated to be 0.6% (25). We note that we observe no significant differences in volatility patterns between matrix that could reflect minor CAI contamination (i.e., with slight enrichments in LREE) in its REE patterns and matrix that does not (Fig. S9). Allende chondrules and matrix record nearly identical REE patterns relative to unaltered CV chondrites, the exception being a slight LREE enrichment for the matrix and perhaps a complementary effect in the chondrules. The Eu anomaly in the chondrules is positive, rather than negative and is somewhat depleted in the matrix relative to unaltered CV matrix, suggesting mobilization of Eu towards the chondrules and LREE leaching from chondrules to matrix. Chondrules from the altered CM chondrite Cold Bokkeveld have REE patterns that are LREE depleted towards CI composition relative to CV chondrules. HREE abundances are on average 3×CI. The overall REE pattern behaves convex upward towards HREE, but has a significant depletion in Eu. These patterns are similar to chondrules from other moderately altered CM chondrites (26) and are attributed to fluid-rock interactions. The Cold Bokkeveld matrix REE pattern is relatively flat with a positive Eu anomaly. The matrix REEs are 1.5-2×CI. Compared to the relatively unaltered CM chondrite Maribo, chondrule and matrix REE patterns of Cold Bokkeveld are enriched, which we suggest is the result of leaching of REEs from CAIs towards the rest of the chondrite during fluid-rock interactions. Maribo chondrules exhibit a reversed convex REE pattern, in which the LREE (La and Ce) are more enriched (1.5-2×CI) than the HREE, which in turn are close to CI composition. The Maribo matrix is similar to CI chondrites and has a slightly positive Eu anomaly. Maribo Ch8 has REE patterns for chondrules and matrix, which appear complementary and are more similar to Cold Bokkeveld than to the other Maribo chondrules. This is also evidenced by the volatility patterns of Ch8 (Fig. 3, main text). We suggest that Ch8 represents a more altered clast within the Maribo chondrite. Two chondrules from CR chondrite NWA801 plot around CI-chondrite composition, in agreement with previous CR chondrule analyses (27). One chondrule (Ch2) is significantly enriched relative to CI, probably because of an overestimation of the Mg abundance, due to abundant Fe metal inclusions within the chondrule. Two out of three chondrules display a dip in Eu and an enrichment of HREE relative to LREE consistent throughout the chondrules (Fig. S11), reminiscent of altered CM chondrule REE patterns, but less pronounced. This might reflect the the relatively mild degree of aqueous alteration in CR compared to CM chondrites. The matrix REE pattern of CR chondrites is fairly flat and ranges from CI-like to 5×CI, unlike CM and CV matrix, which is on average CI-like. This suggests that the CR chondrite matrix is more thermally processed.

Individual volatility patterns. This section will focus mainly on the volatility patterns of individual chondrules, since the compositions of the matrices are discussed at length in the main paper. Volatility patterns of individual chondrules of CV chondrites are consistent within a chondrule (Fig. S13), reflecting the reproducibility of our data, but also between CV chondrules with different petrologies and from different chondrites with a similar degree of alteration (Fig. S14). For example, we have analyzed porphyritic olivine chondrules and barred chondrules from Leoville and Vigarano, yielding very similar patterns (Fig. S17). Such similarity requires a generic chondrule formation process that results in similar chondrule compositions, but with variable textures. Chondrules textures have so far been ascribed to either (1) different peak temperatures and cooling rates (28) or (2) the presence of nucleation sites (e.g., micrometer-sized metal blebs) in chondrule melts from heterogeneous precursor materials (29). In detail, during chondrule formation, the surrounding volatile-rich gas is absorbed by a Ca,Al-rich refractory melt. Through diffusion, olivines start to grow, resulting in either seeded, porphyritic or non-seeded barred textures.

In this model, the bulk composition of chondrules is controlled by the duration of gas-melt interaction and the partial pressures reigning in the gaseous environment (29). Most of the chondrule composition (60-70%) is derived from the gas-phase and variations in chondrule bulk composition are the result of heterogeneous accretion of chondrule precursor material, rather than of chondrule formation processes such as evaporation. Although CV chondrules with different textures show very similar volatility patterns, the only marked difference is that barred chondrules appear to have a lower Fe abundance. Considering the models discussed above, this could reflect 1) more Fe metal expulsion during chondrule formation related to higher peak temperatures of barred chondrules or perhaps the faster cooling rates, which do not allow for recondensation of Fe onto the chondrule or 2) a lower abundance of Fe metal to start with. Hence, our data does not distinguish between models that account for different chondrule textures. The use of isotope tracers such as Mo or W that are carried in the metal phase may be more successful. Either way, the similarity of CV chondrule volatility patterns suggests either formation of these chondrules from the same spatiotemporal reservoir, or a generic chondrule formation process for chondrules of this size. Since Pb-Pb ages, Mg and Cr isotope data of individual CV chondrules suggest that they originate from different reservoirs and times (30, 31), it may well be the latter. However, age and isotope data are needed for the chondrules in this study to confirm this. The rims of porphyritic CV chondrules B-ch1 and A-ch2 are rich in low Ca pyroxene relative to the chondrule cores and contain a higher phenocryst/mesostasis ratio and a higher abundance of Fe sulfides. The volatility patterns of these rims are generally more volatile-rich (at condensation temperatures <1300 K) and in case of A-ch2 more CI-like regarding the refractory plateau (Fig. S13). Within these patterns, enrichments of Sr and U can be observed, similar to CM chondrule patterns (Fig. 3, main text, Fig. S15). In sum, the volatility patterns of the CV chondrule rims are intermediary between CV and CM chondrules. The rims are likely more CI-like than the cores, because of a higher level of interaction with the gas. In the main text, we proposed that the relatively small size of CM chondrules is key to obtain CI-like volatility patterns, due to a higher degree of re-absorption from the surrounding volatile-rich gas. The petrology and size of CV and CR chondrules is very similar, both containing a majority of type I PO chondrules and having average sizes of 1.0 and 0.7 mm, respectively (32). The volatility patterns of both chondrule populations are also very similar, with the same average and flat compositions of the refractory plateau, which are 2-3×CI (Fig. S13), and similar depletions in siderophile elements. Nevertheless, the volatile depletion of CR chondrules is an order of magnitude larger than for CV chondrules. This implies an additional volatile loss of CR chondrules, perhaps due to the recycling of these chondrules (27). The last remelting event of CR chondrules may have produced the observed complementarity between chondrules and matrix.

Mass balance equations in a three-component system. A first order observation of our data in figure 1 of the main text is that Leoville matrix has a higher Fe/Mg ratio than Maribo matrix. This is completely attributed to an increase in Fe in the matrix, since Leoville and Maribo matrix lies vertically above the CI composition in figure 1A. The expectation is then, that Leoville should have a higher abundance of metal to account for the enrichment of Fe in the matrix. Indeed, CV chondrites have 0-5 vol.% metal and 30 vol.% of matrix, relative to 0.1 vol.% metal and 70 vol.% matrix in CM chondrites (32). NWA801 matrix plots near Maribo matrix, whereas NWA801 relatively contains much more metal. However, NWA801 is likely more altered (type <2.6, 8) than Maribo and hence, the matrix composition may have shifted to being more Mg-rich and, thus, Fe/Mg-poor. We will, therefore proceed with mass balance calculations of CV and CM chondrites, since the extent of Fe transfer through secondary alteration in CR chondrites is unknown.

The usual argument against mass balance calculations between chondrules and matrix is that the initial abundance of matrix and chondrules is unknown (33). This is how elemental ratio plots with completely skewed mass balances compared to observed volume abundances are justified (14). Note that these calculations are usually referred to as 'mass balance equations', whereas we are actually looking at a 'volume balance'. Since the density variation between CV chondrules and matrix is not large (34), it may not matter as much in these models, but in a three-component model taking into account chondrules, metal and matrix, we need to consider the density, since the density of metal is 3 times larger than CI chondrites.

CV chondrites: The mass balance for Leoville matrix is as follows: the Fe content of the matrix (36.5 wt.% Fe on average, see Figure 1 of the main text) is a mixture between approximately 83 wt.% CI (containing 19 wt.% Fe) and 17 wt.% metal (assuming 100 wt.% Fe for simplicity). Note that we carry out these mass balance equations with Fe in its reduced form. Assuming a density of 7.87 g/cm^3 for pure Fe metal (slightly lower if containing Ni) and a density of 2.42 g/cm^3 for CI chondrites (35), then ∼6 vol.% metal is contained in the matrix of the dust rims. Hence, only a small addition of metal is needed to explain the Fe/Mg ratios of the matrix, especially considering that the volume abundance of individual dust rims matches the metal rims (Fig. S19). The volume abundance of metal in the matrix corresponds to 1.8 vol.% metal in the bulk CV chondrite, assuming 30 vol.% matrix (32). We note that this abundance should be lower, if the intra-chondrule matrix has lower Fe/Mg ratios than the dust rims, since the dust rims do not contain all of the matrix in CV chondrites. Another limitation to the mass balance equation is that in our model, it is also possible that metal erosion to the surrounding matrix occurred before accretion to the chondrite parent body and that the original dust rim was much bigger. In that case, as illustrated in Figure S19, the relative transfer of metal to the matrix must have been larger. However, the amount of metal transferred to the matrix is still small relative to the volume abundance of the metal rim. One would have to make the original dust rim dis-proportionally large to reach the same amount of metal in the matrix as is present in the metal rim.

We also regard the maximum amount of metal that was expelled from the chondrules. If the calculated amount of metal in the dust rims exceeds the maximal abundance of expelled metal, then our model is not valid. This information can be taken from the volatilityatterns of the chondrules, where we observe Fe depletion as a result of evaporation and metal expulsion

Elishevah van Kooten, Frédéric Moynier and Arnaud Agranier

during chondrule formation. In Figure S20, we give an example of the average Leoville chondrule. If we compare the amount of Fe in a model chondrule without metal expulsion and only Fe loss through evaporation (e.g., similar to Mg), then the amount of Fe in the chondrule would be 1.5 × CI, which amounts to 27.5 wt.% of Fe. After metal expulsion from the averaged Leoville chondrules, the amount of Fe in the chondrules is 0.2 × CI, which corresponds to 3.7 wt.% Fe. Normalizing the Fe content of the original chondrule, this means that we would have had $(27.5\text{-}3.7)/(100\text{+}27.5) \times 100 = 22.2$ wt.% Fe in the initial chondrule, after evaporation, but before metal expulsion. This means that we lost 22.2 - 3.7 = 18.5 wt.% Fe from the chondrule during metal-silicate separation. This is equivalent to about 10 vol.% of metal lost from the chondrules, which corresponds to 5-6 vol.% of the bulk CV chondrite if we assume 50-60 vol.% CV chondrules (Scott and Krot, 2007). This is in agreement with observations from CV chondrites, which show <5 vol.% metal in bulk CV chondrites. Since the total calculated metal abundance in the matrix is <1.8 vol.%, our mass calculations show that the amount of metal expelled from the chondrules can account for the observed metal in the chondrules and the inferred metal abundance in the matrix. The calculated mass transfer from metal to matrix, would be <30%.

CM chondrites: The mass balance of Fe in Figure 1A (main text) yields 7.4 wt.% metal versus 93.6 wt.% CI-matrix, corresponds to 3 vol.% metal in the dust rim matrix and 1-2 vol.% in the bulk CM chondrite, assuming a matrix content of 30-70 vol.%. The matrix content in CM chondrites is officially about 70 vol.% (Scott and Krot, 2007), but this is including tochilinite-cronstedtite intergrowths (TCIs), which should not be considered part of the matrix. In Maribo, TCIs contain their own dust rims. Without TCIs, we estimate the matrix abundance to be approximately 30 vol.%, which is similar to CO and CV chondrites. The CM chondrules contain a Fe abundance of 0.6 × CI, whereas the abundance before metal expulsion, but following volatile evaporation, is estimated to be 2 × CI, which amounts to 11 wt.% and 37 wt.% of Fe, respectively. The amount of Fe before metal expulsion is difficult to estimate; since CM chondrules reabsorbed their lost volatiles to greater extent than CV chondrules (see main text for further explanation). This of course greatly affects the calculated amount of Fe lost during metal-silicate separation. Normalizing the Fe content of the original chondrule, this means that we would have had $(37\text{-}11)/(100\text{+}37) \times 100 = 19$ wt.% Fe in the initial chondrule, after evaporation, but before metal expulsion. This means that we lost 7 wt.% Fe from the chondrule. This is equivalent to about 3.6 vol.% of metal lost from the chondrules, which corresponds to 0.36 vol.% of metal in the bulk chondrite when assuming 10 vol.% chondrules (2). The observed metal in CM chondrites is about 0.1 vol.%, which is in good agreement with our calculations considering their limitations as outlined above. In the most unaltered CM chondrites Paris, much higher metal abundances are observed (<3 vol.%, 3), but it is unclear whether this is related to heterogeneous accretion or lack of secondary alteration (3, 4). In Maribo, the unaltered CM chondrite from this study, the observed metal abundance matches the metal content observed in more altered CM chondrites when looking at the chondrite by EMP. However, unlike the more altered counterparts, small metal nuggets are observed in the dust rims, only observed by TEM (4). These metal nuggets are estimated to comprise up to a few vol.% of the Maribo matrix and could, hence, account for the Fe/Mg ratios in this chondrite. Within the limitations of the mass balance equations, the metal in the dust rims could be derived by mass transfer from the chondrule metal rims since calculated metal expulsion could be similar to the inferred metal contribution to a CI-like matrix. However, these calculations do not rule out that the metal in Maribo matrix does not necessarily have to be derived from the adjoining chondrules, but may have accreted together with the matrix.

50% Condensation temperature (K)	Isotope
1741	91Zr
1684	178Hf
1659	89Y
1659	160Gd
1659	159Tb
1659	161Dy
1659	165Ho
1659	167Er
1659	175Lu
1659	232Th
1610	238U
1602	146Nd
1590	147Sm
1582	49Ti
1582	141Pr
1578	139La
1573	181Ta
1559	93Nb
1517	43Ca
1487	173Yb
1478	140Ce
1464	88Sr
1455	138Ba
1356	151Eu
1353	60Ni
1352	59Co
1336	25Mg
1334	57Fe
1296	53Cr
1158	55Mn
800	85Rb
799	133Cs
727	208Pb

Table S1. Isotopes analyzed by LA-ICPMS and their corresponding 50% condensation temperatures ([15]).

Elishevah van Kooten, Frédéric Moynier and Arnaud Agranier
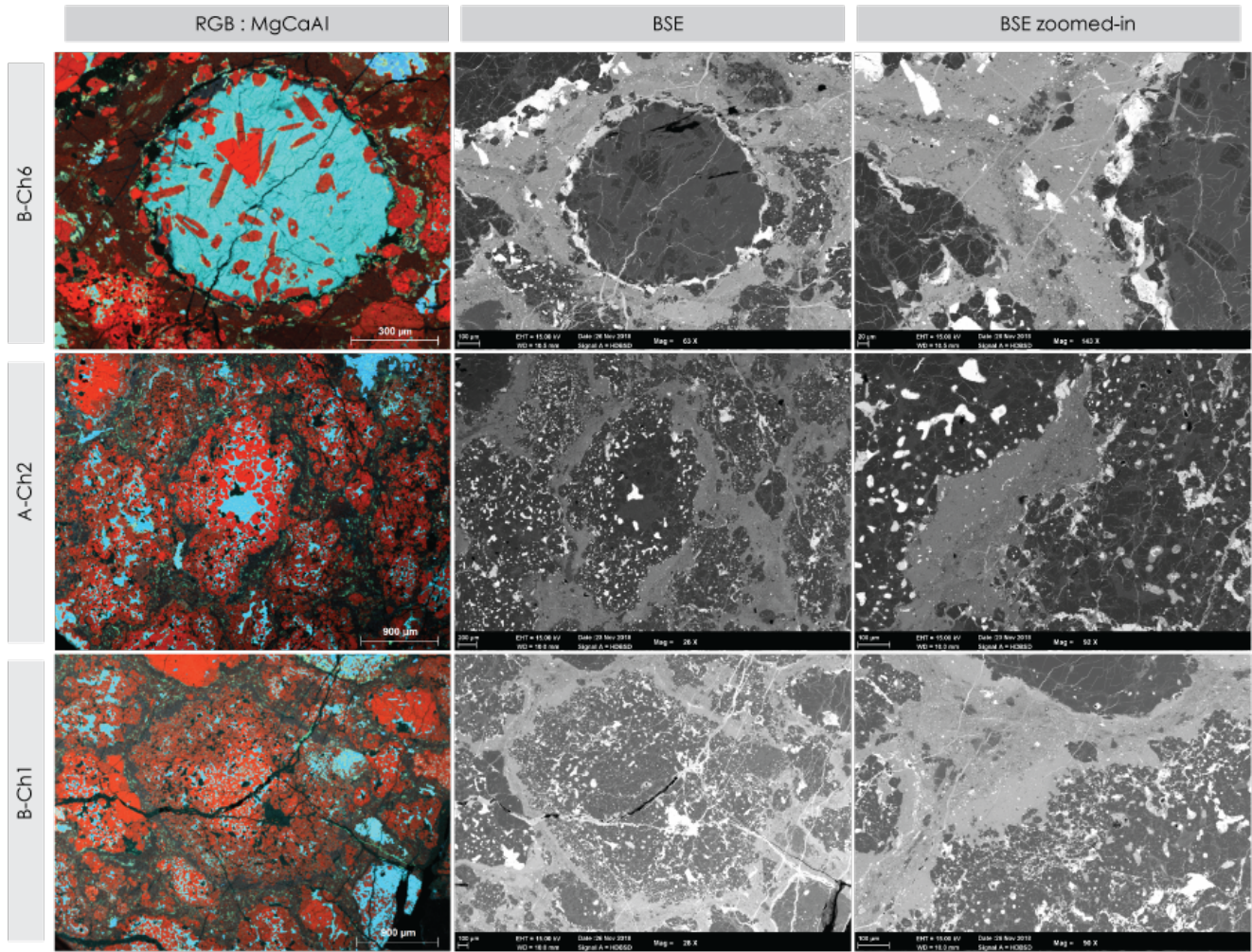
Fig. S1. MgCaAl elemental maps and BSE images of three Leoville chondrules.
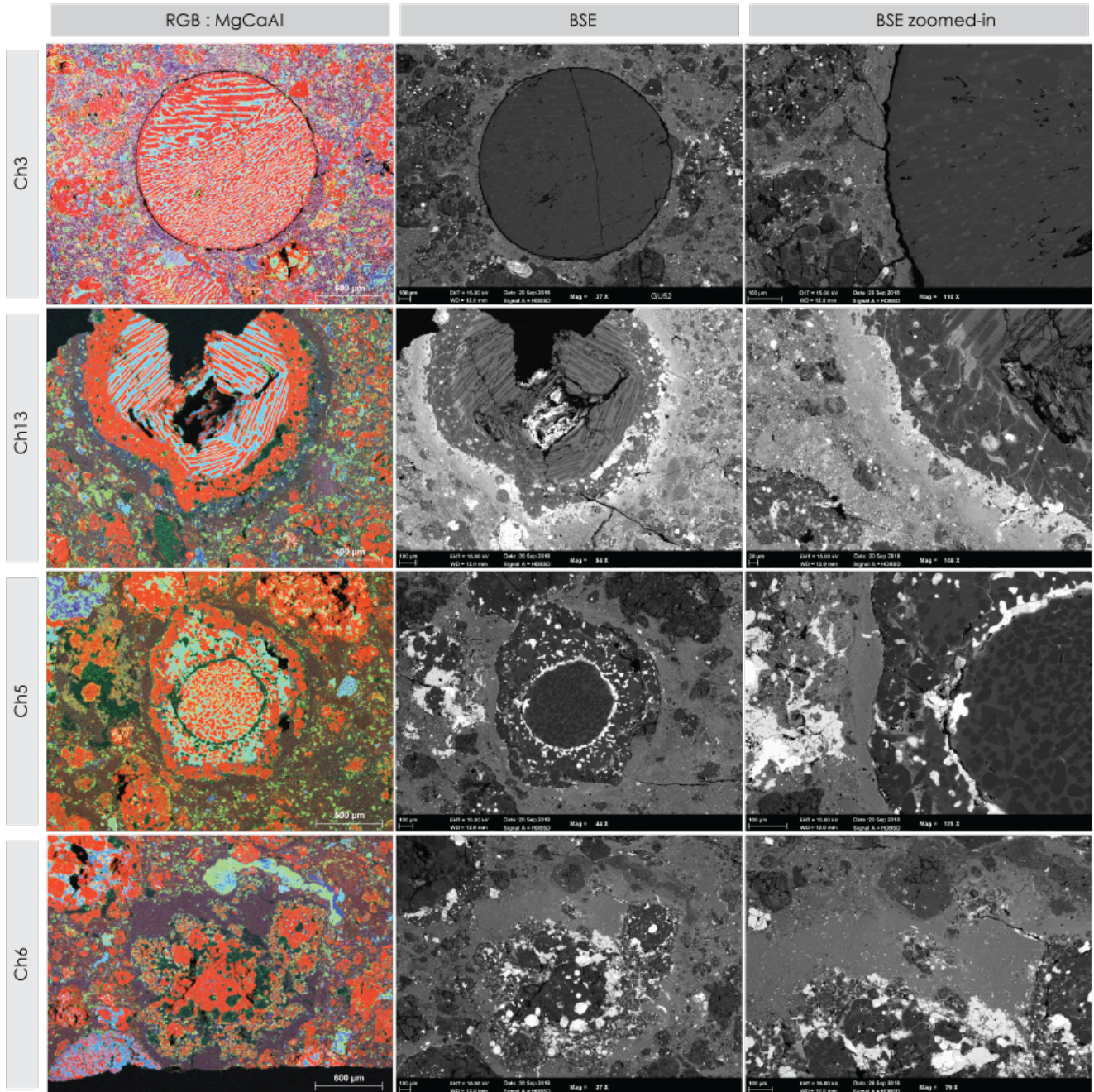
Fig. S2. MgCaAl elemental maps and BSE images of four Vigarano chondrules.

Elishevah van Kooten, Frédéric Moynier and Arnaud Agranier
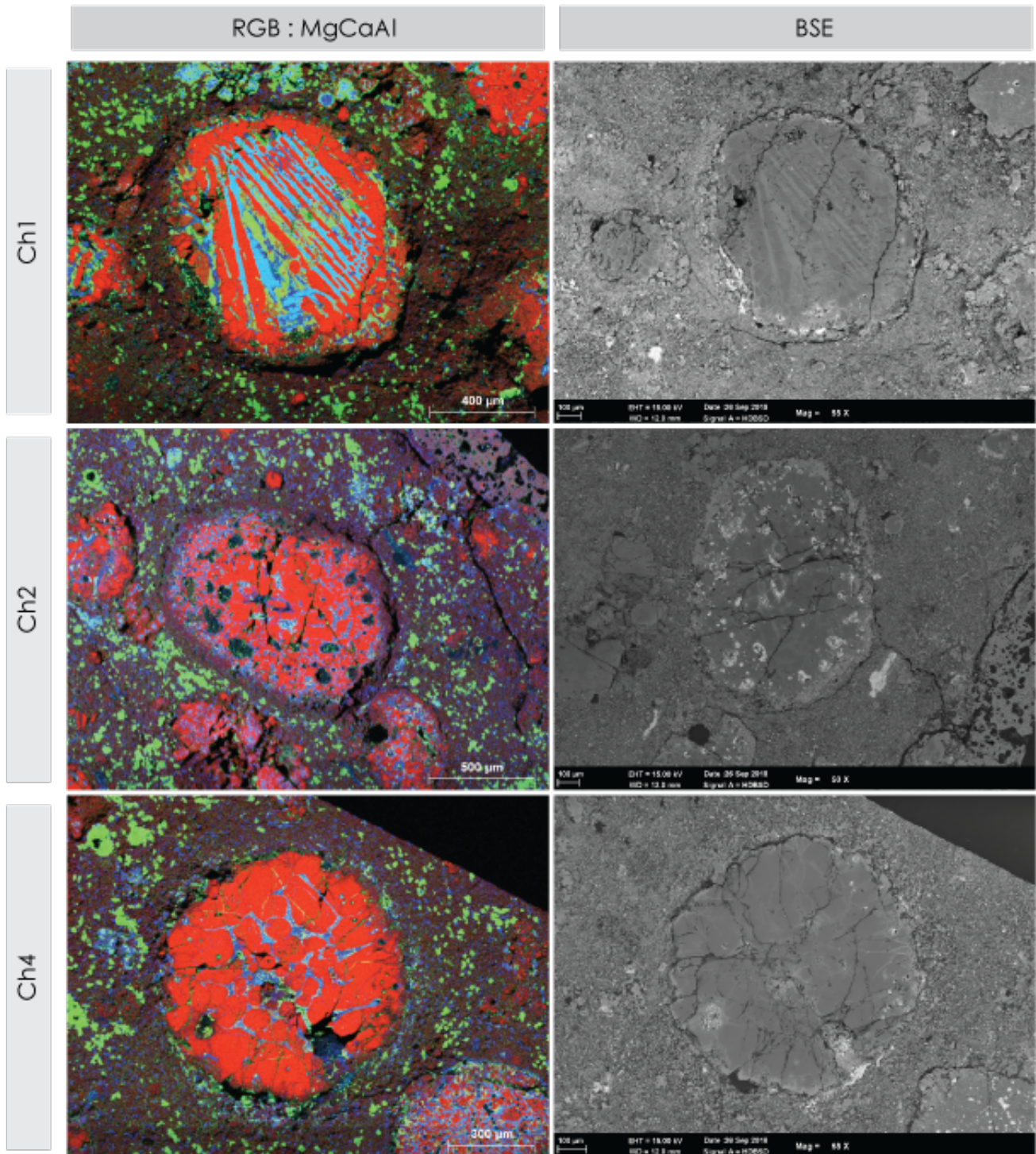
Fig. S3. MgCaAl elemental maps and BSE images of three Allende chondrules.

RGB : MgCaFe	BSE
Ch1	
Ch4	
Ch8	
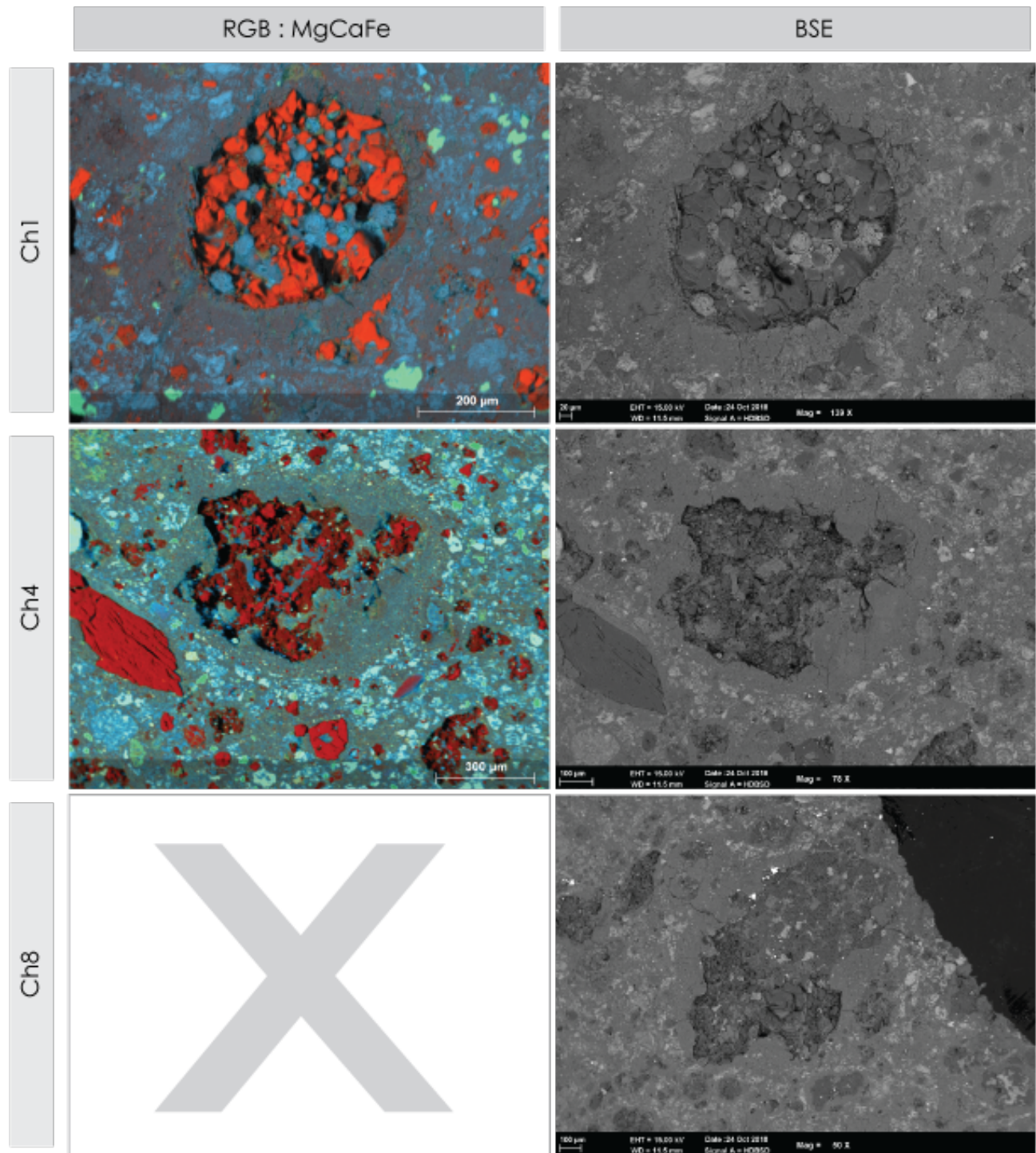
Fig. S4. MgCaAl elemental maps and BSE images of three Maribo chondrules.

Elishevah van Kooten, Frédéric Moynier and Arnaud Agranier
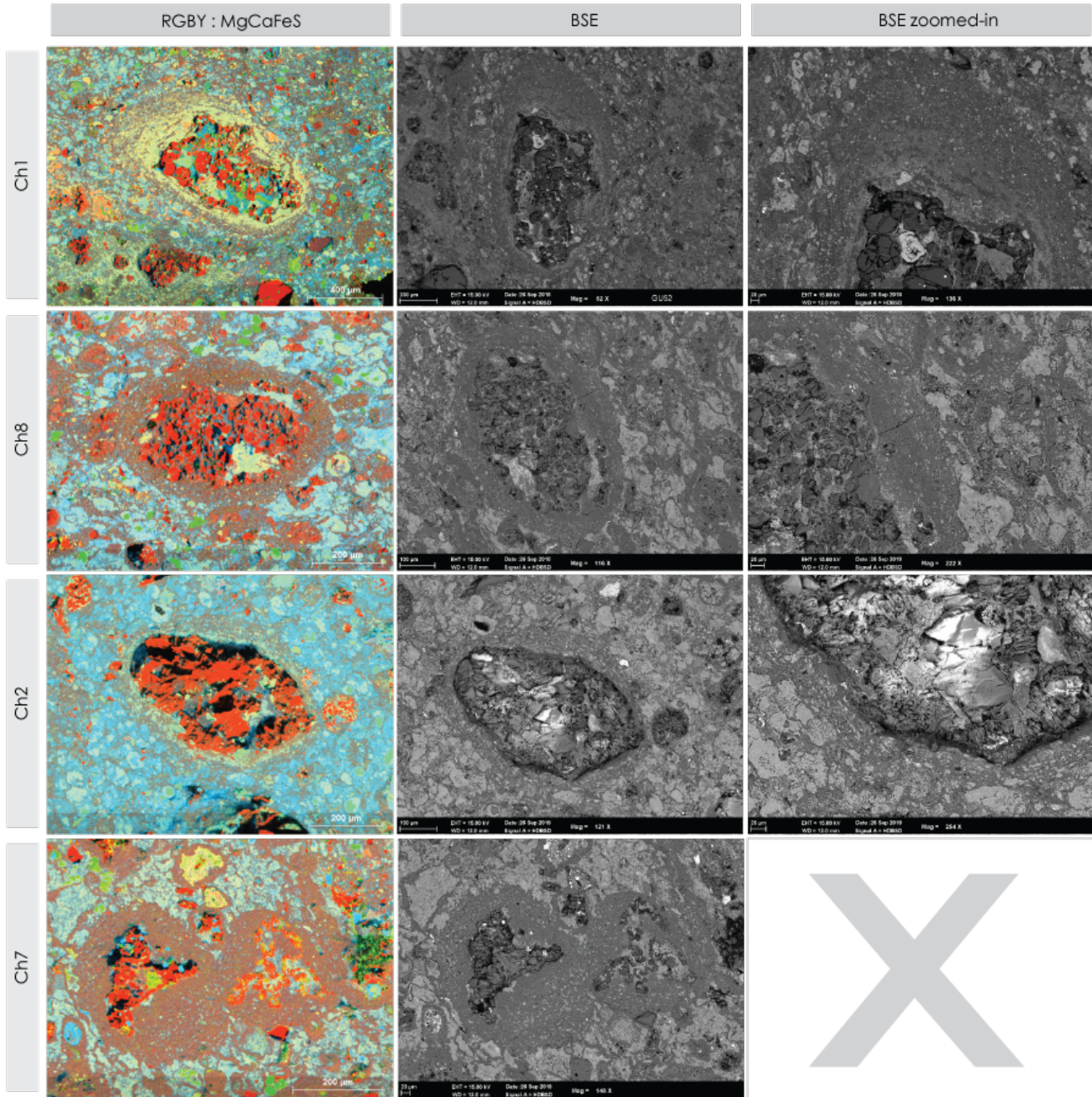
Fig. S5. MgCaAl elemental maps and BSE images of four CM chondrules from Cold Bokkeveld.
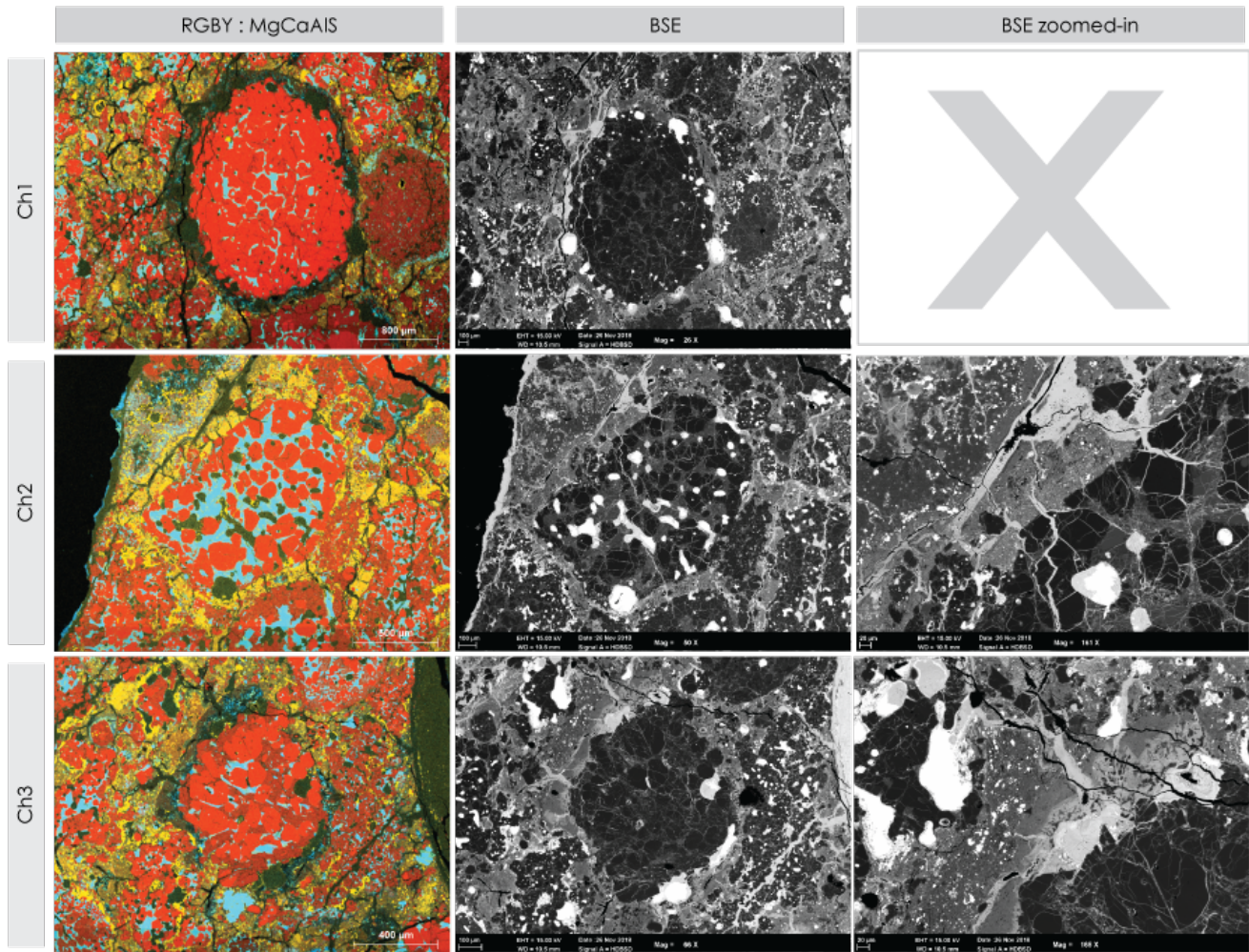
Fig. S6. MgCaAl elemental maps and BSE images of three CR chondrules from NWA801.
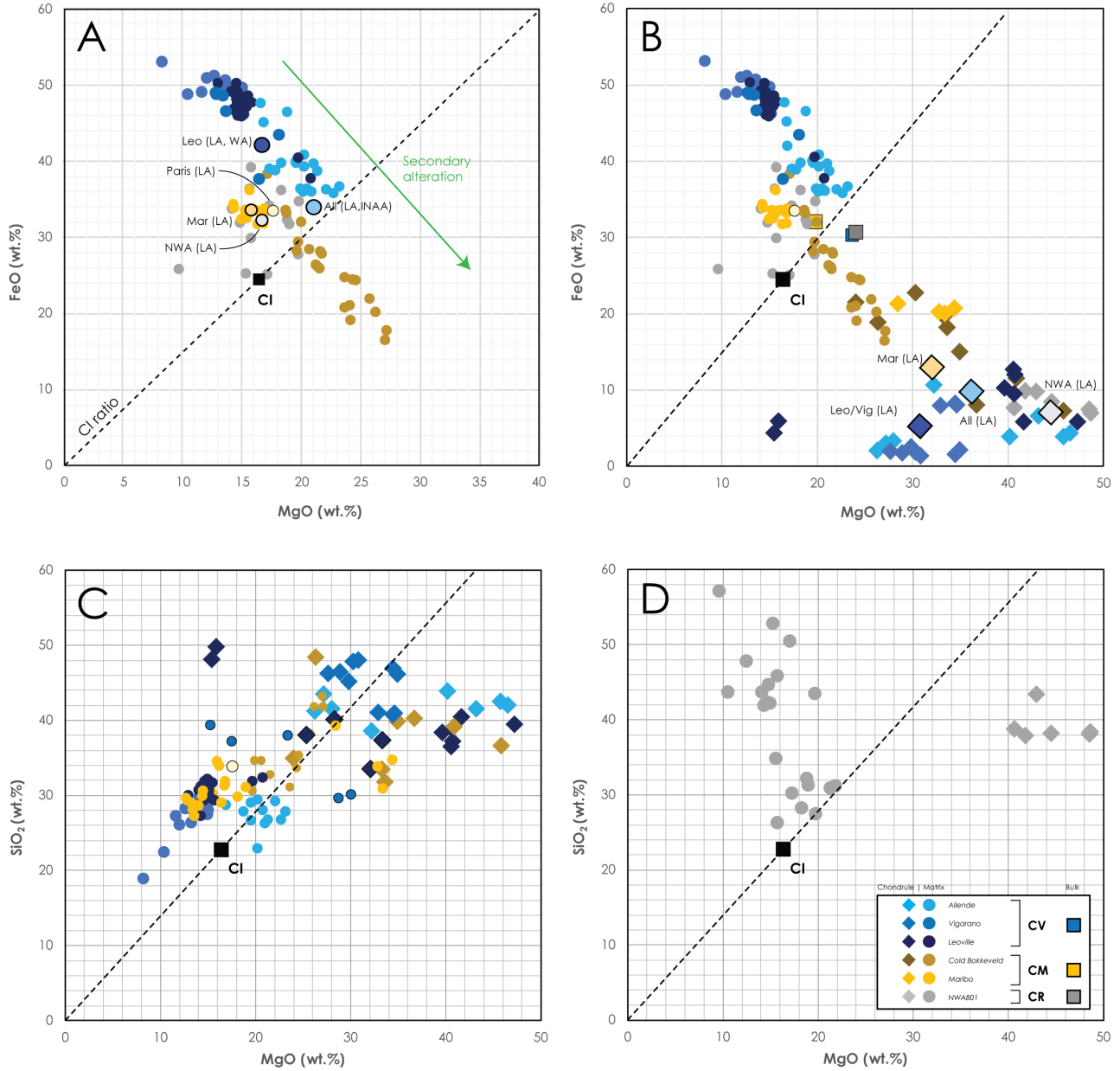
Fig. S7. Fe, Mg and Si concentrations for CV, CM and CR chondrite matrix and chondrules, identical to main text Figure 1 with addition of LA-ICPMS, wet analyses and INAA data from literature (3, 36–39). C) SiO₂ versus MgO wt.% of chondrules and dust rims from CV and CM chondrites, which all plot on or near the CI ratio line, showing limited fractionation of Si and Mg during chondrule formation. D) The same plot as panel C, but for CR chondrite NWA801, clearly deviating from the CI ratio line.
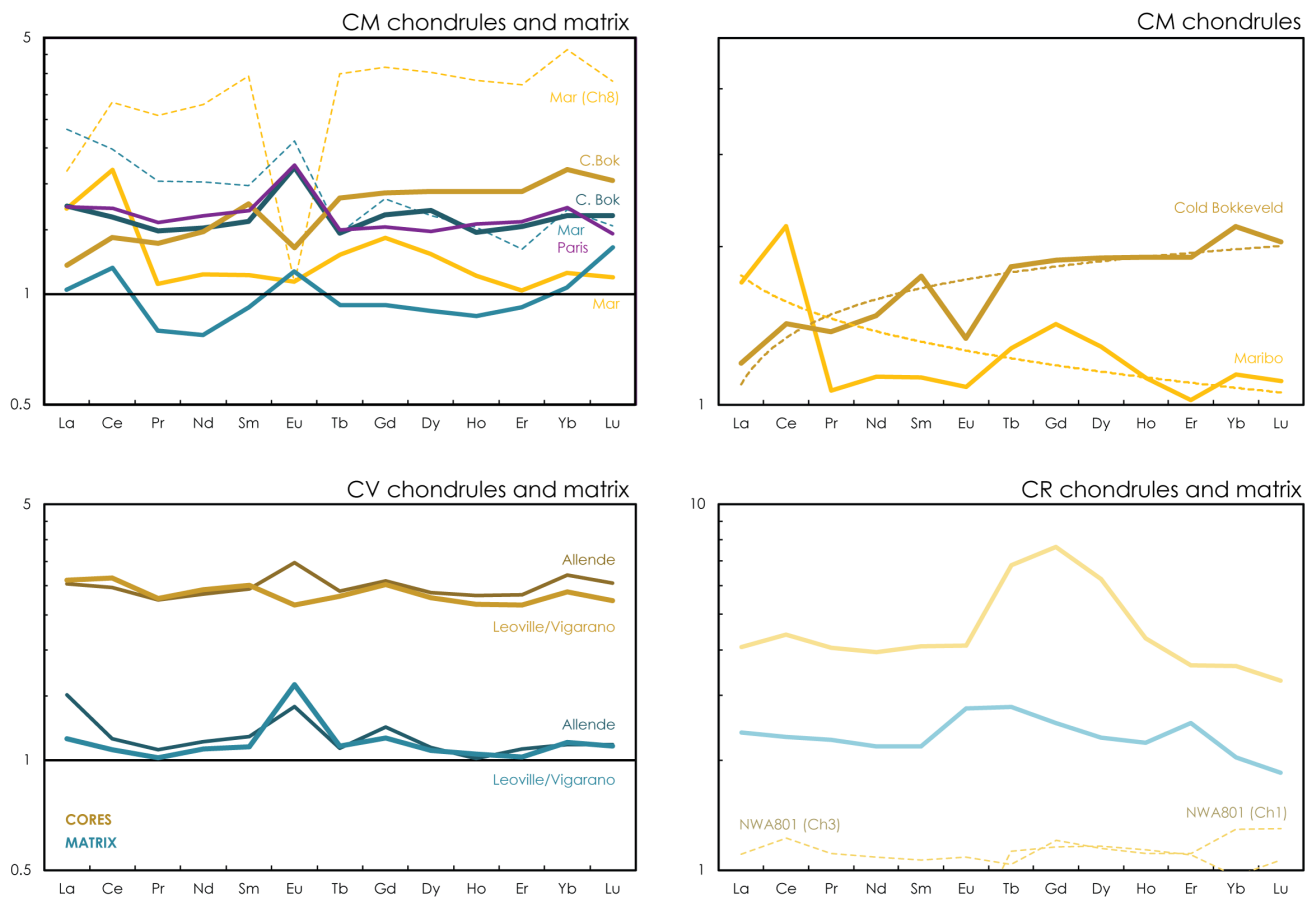
Fig. S8. Averaged REE patterns of CM, CV and CR chondrules and matrix, normalized against CI composition.
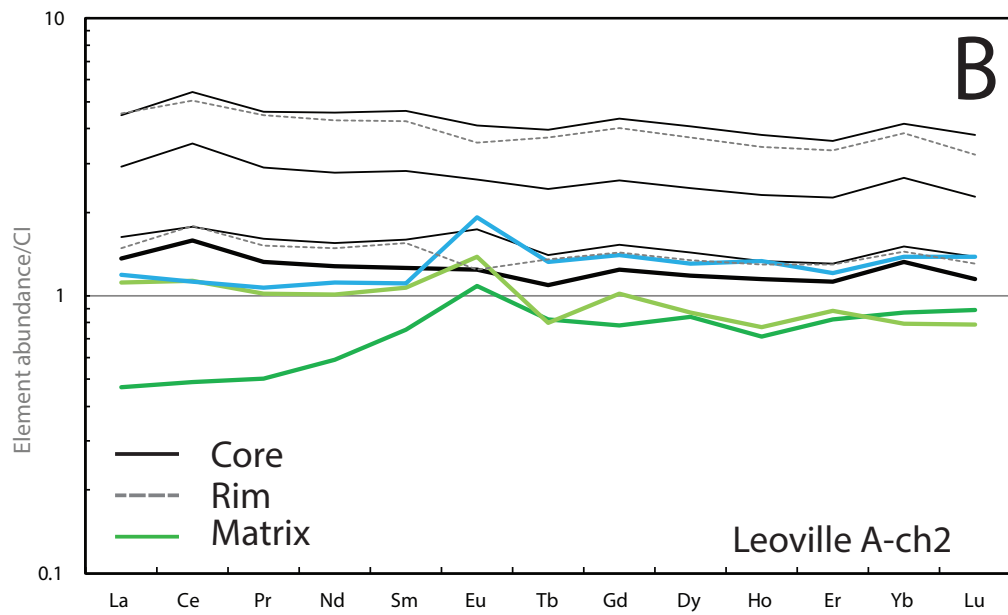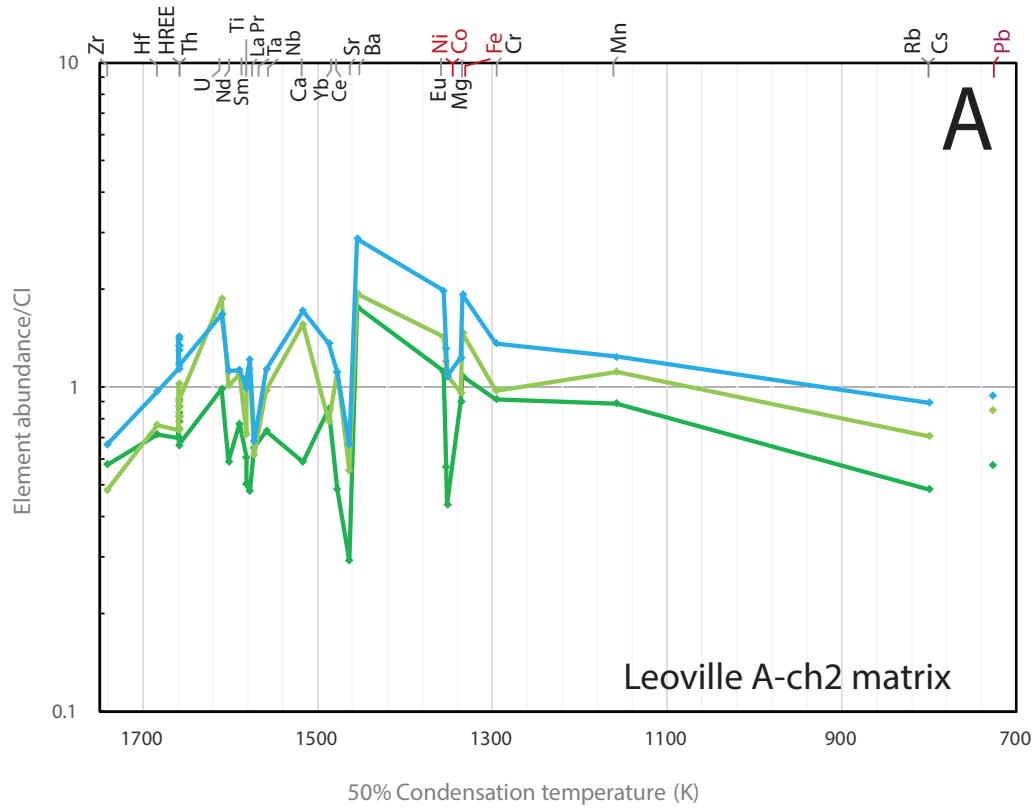
Fig. S9. A) Individual CV matrix volatility patterns from a single dust rim in Leoville and B) Corresponding individual REE patterns of matrix, chondrule core and rim.

Elishevah van Kooten, Frédéric Moynier and Arnaud Agranier
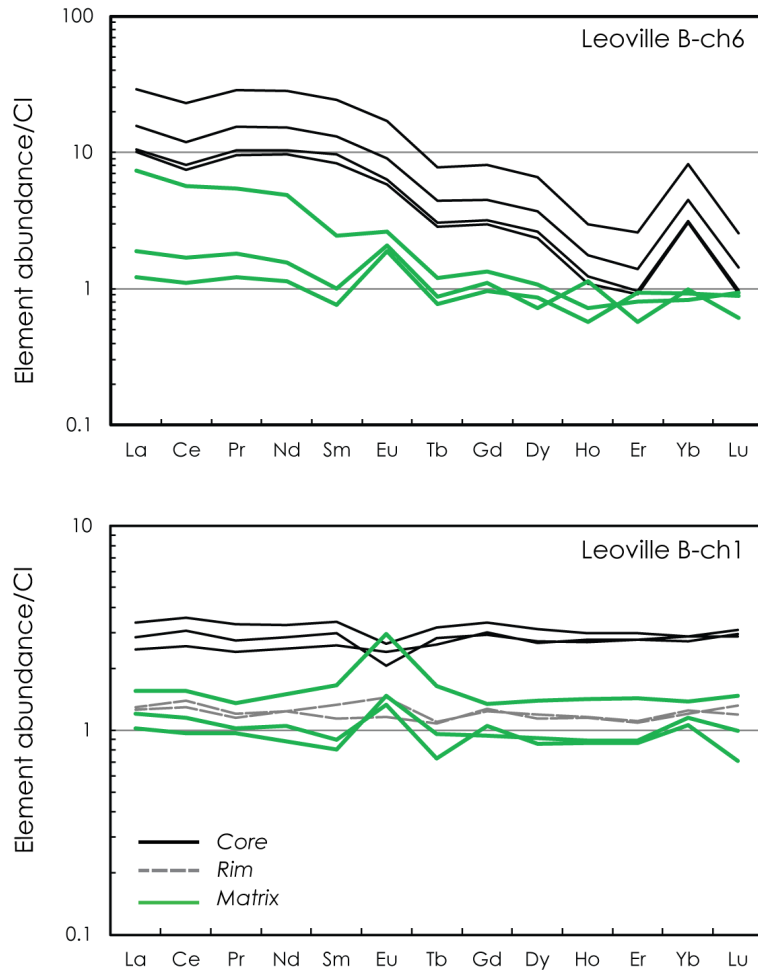
Fig. S10. Individual REE patterns of chondrule cores, rims and surrounding matrix from two Leoville chondrules.
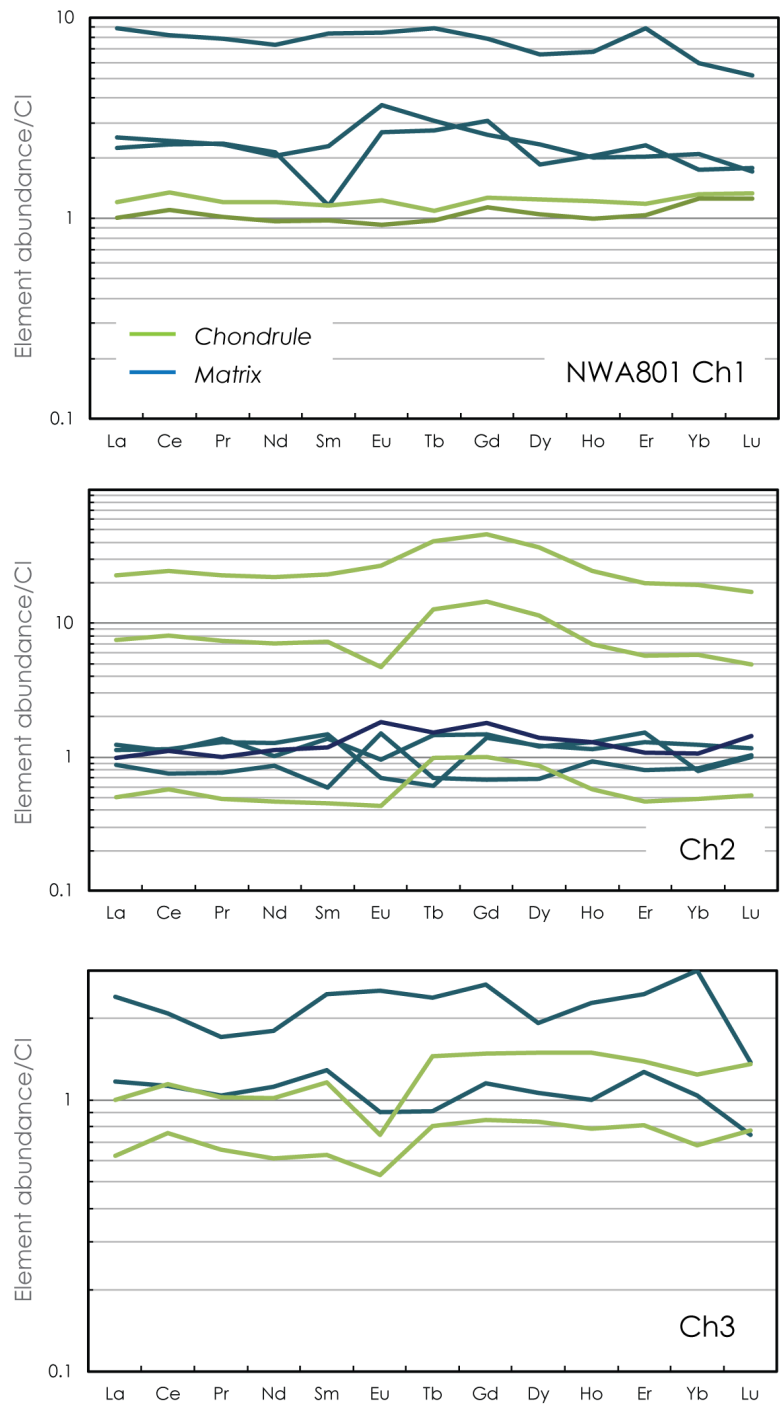
Fig. S11. Individual REE patterns of chondrules and matrix from CR chondrite NWA801.
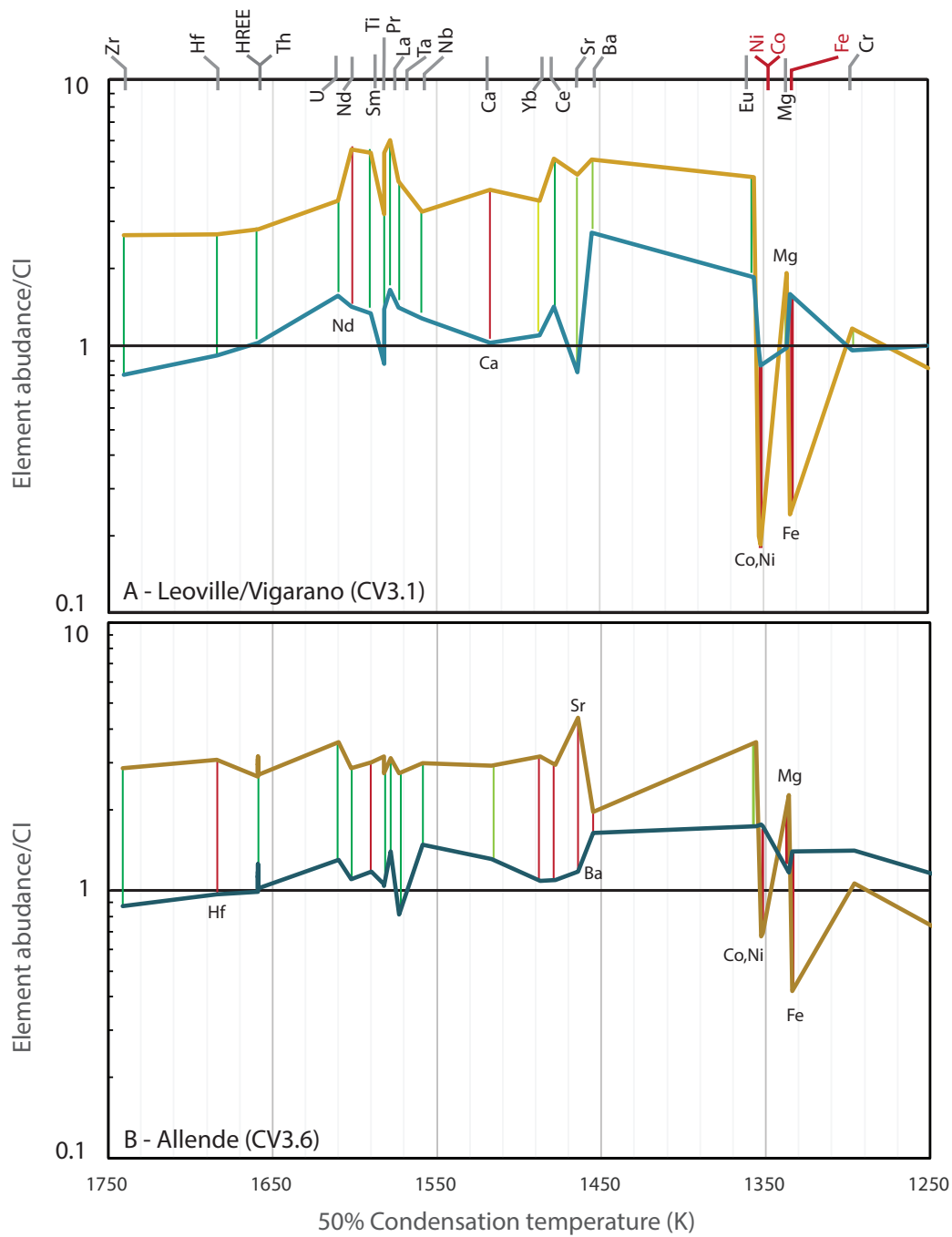
Fig. S12. Averaged volatility patterns of A) Leoville and Vigarano chondrules and matrix and B) Allende chondrules and matrix, with red (non-mirroring) and green (mirroring) connecting lines between chondrule and matrix elemental abundances. Note that with progressive alteration, CV chondrules and matrix become more complementary to each other.

Elishevah van Kooten, Frédéric Moynier and Arnaud Agranier
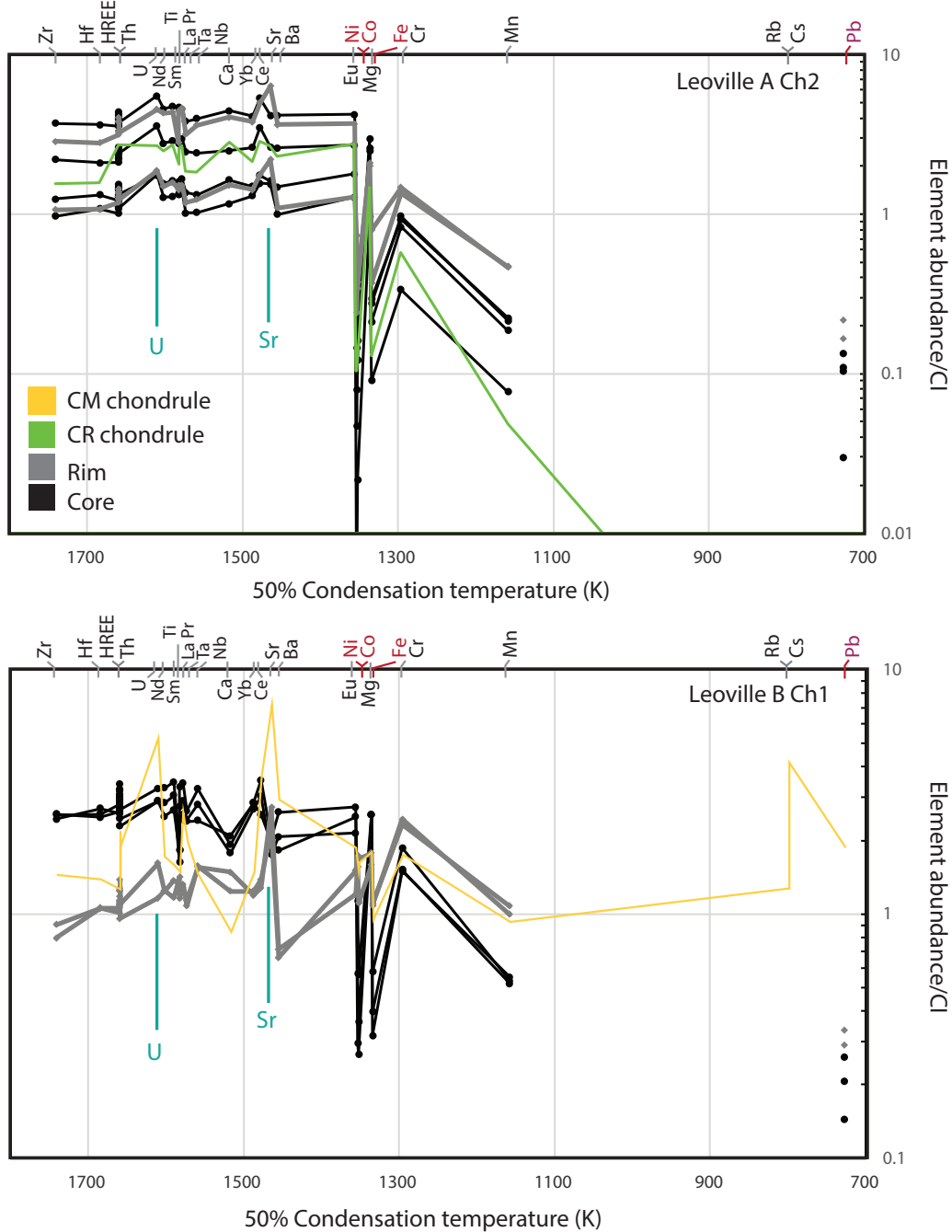
Fig. S13. Individual volatility patterns from two Leoville chondrule cores and rims, along with the average chondrule composition from CR chondrite NWA801 and the average chondrule composition from Maribo.
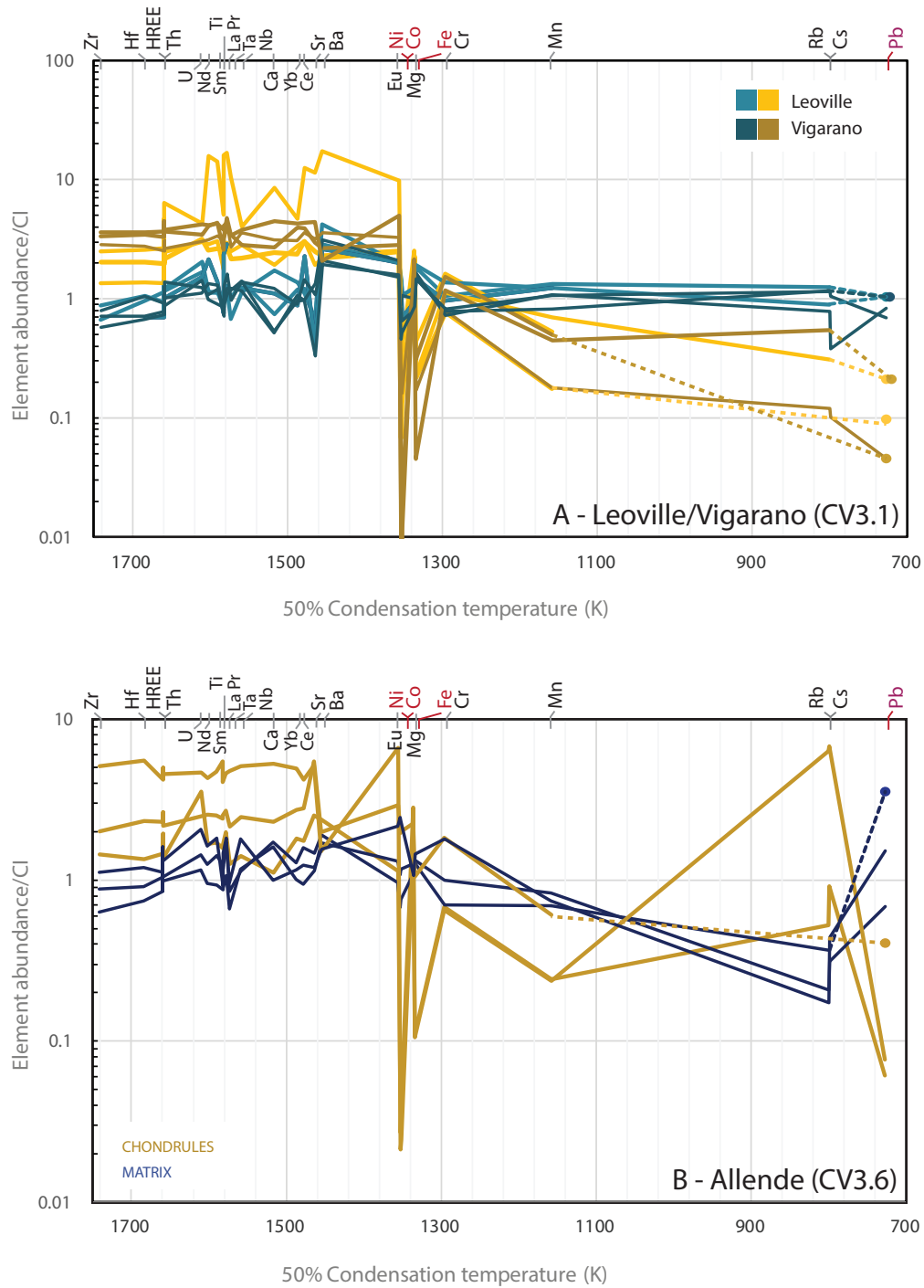
Fig. S14. Averaged volatility patterns of individual Leoville, Vigarano and Allende chondrules and matrix

Elishevah van Kooten, Frédéric Moynier and Arnaud Agranier
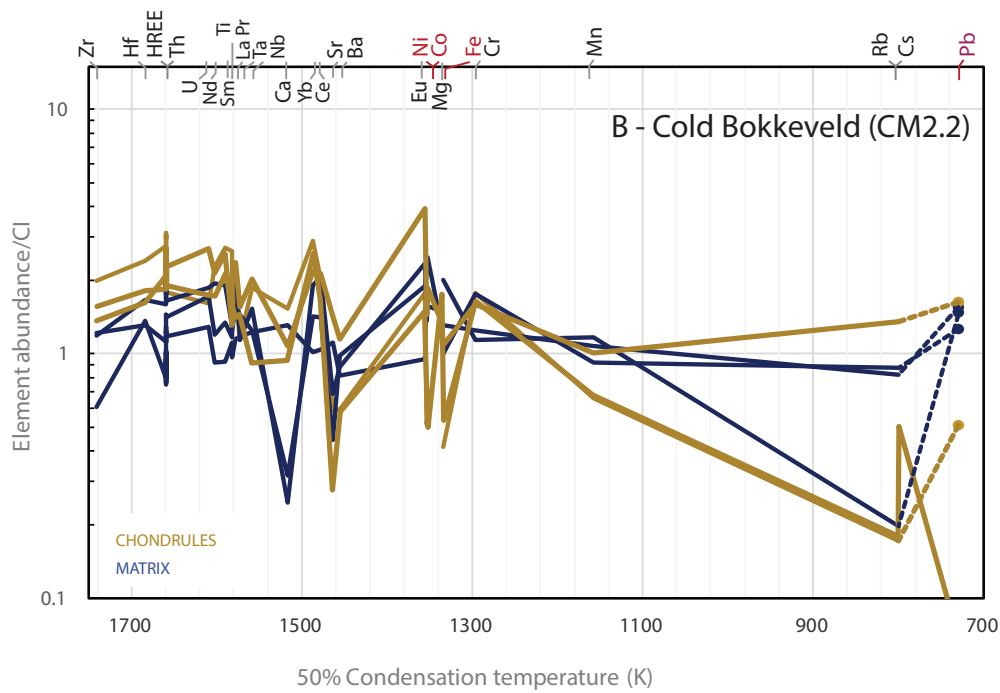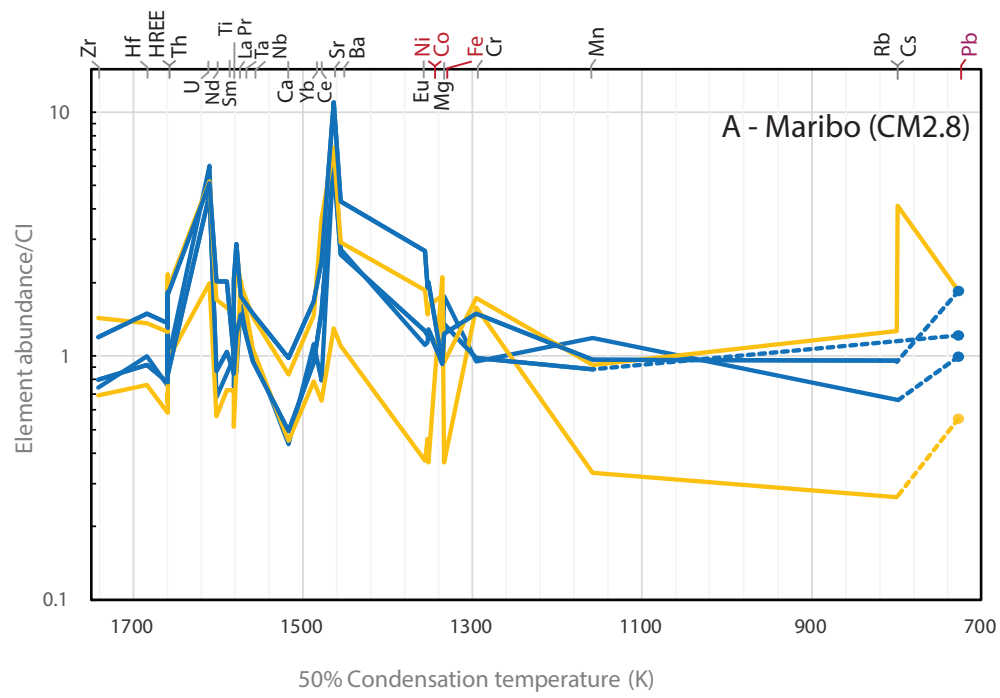
Fig. S15. Averaged volatility patterns of individual Maribo and Cold Bokkeveld chondrules and matrix
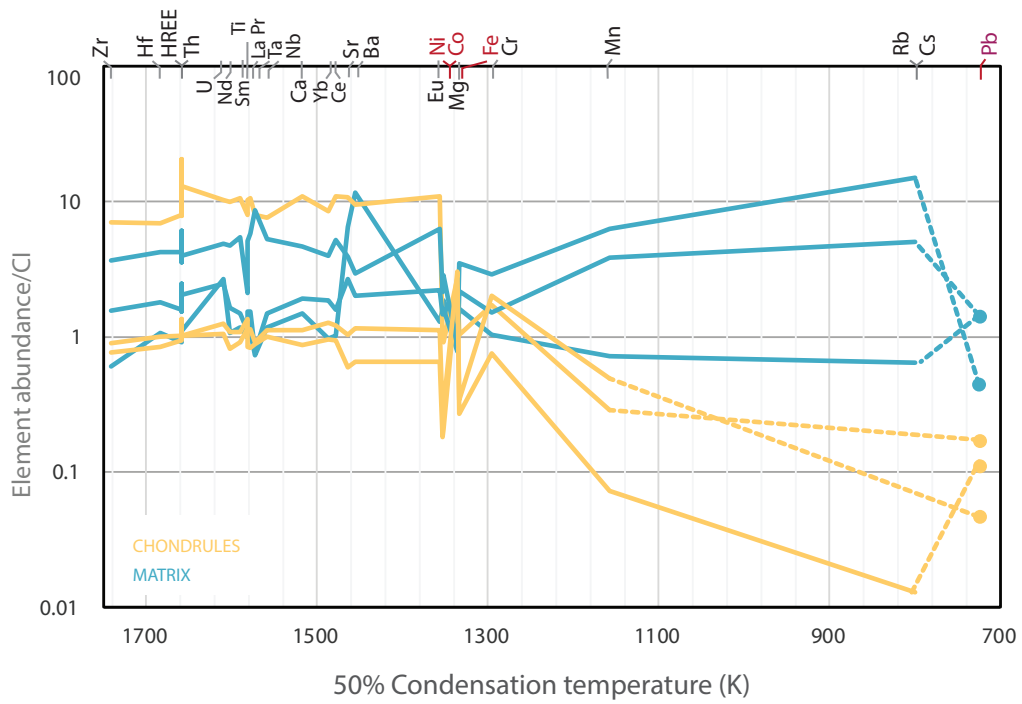
Fig. S16. Averaged volatility patterns of individual NWA801 chondrules and matrix. We note that the refractory plateau of Ch2 is very high relative to CI abundances. This is related to an overestimation of the Mg content in this chondrule, due to a high abundance of FeNi metal. This chondrule is not taken into the average composition of NWA801 chondrules used in Figure 4 of the main text.

Elishevah van Kooten, Frédéric Moynier and Arnaud Agranier
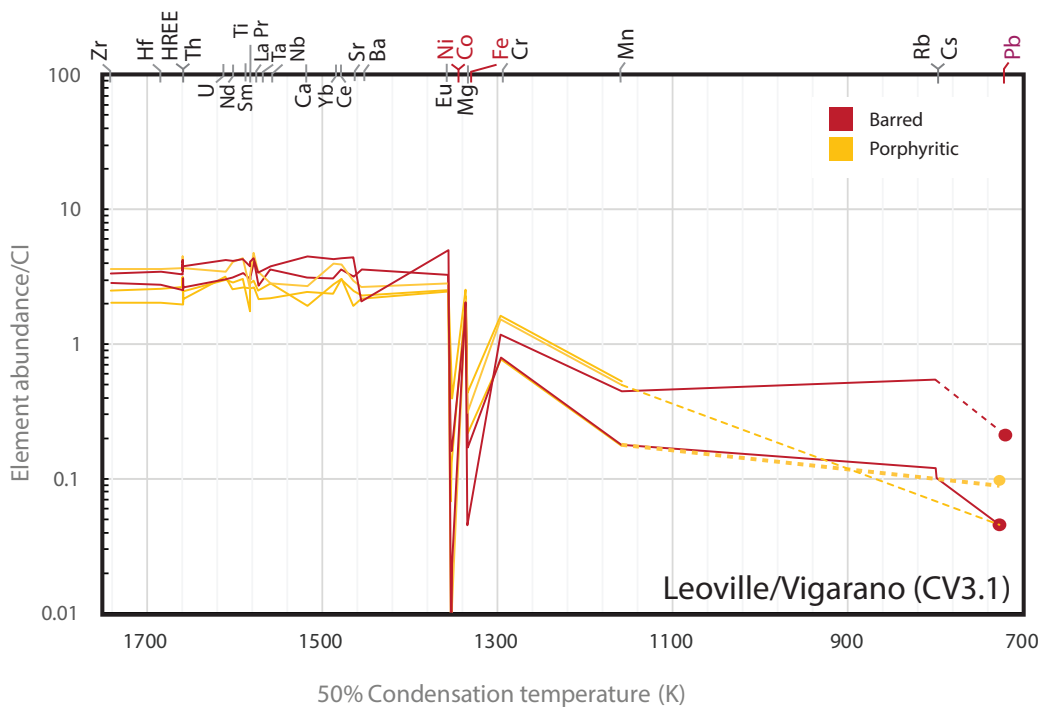
Fig. S17. Volatility patterns from barred and PO chondrules from Leoville and Vigarano.
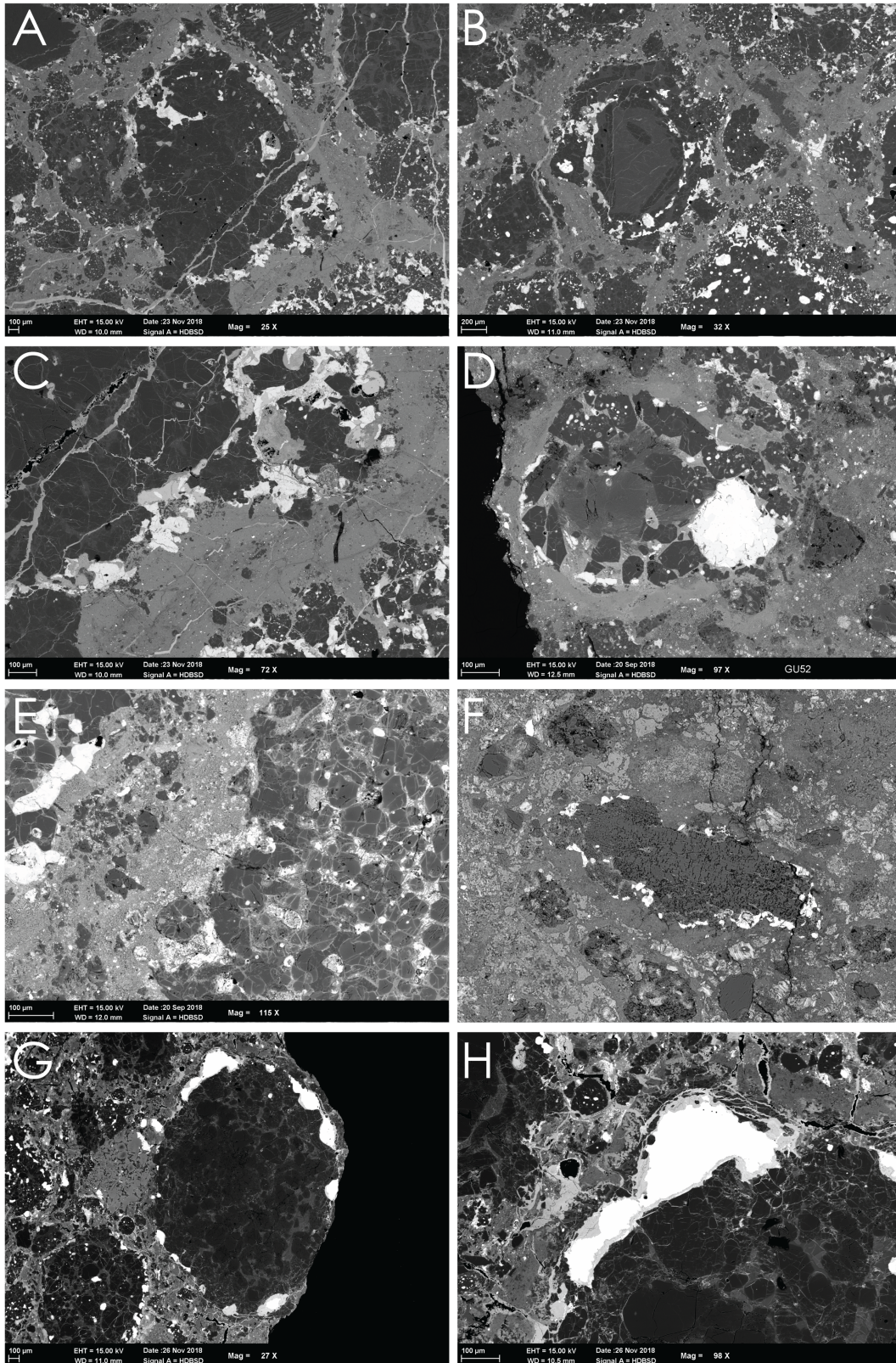
Fig. S18. Armored chondrules from A-C) Leoville, where B) has a primary and secondary metal rim and C) oxidation of metal in contact with surrounding matrix in which small metal beads can be observed; D-E) Vigarano in which D) reflects alteration of chondrule mesostasis and surrounding metal through Fe enrichment from the altered metal rim and E) erosion of metal from the chondrule to the matrix is visible; F) Maribo; G-H) NWA801, where G) shows a typical beaded metal rim, resulting from cooling of the metal on the chondrule and H) oxidation of the metal during early stage aqueous alteration.

Elishevah van Kooten, Frédéric Moynier and Arnaud Agranier
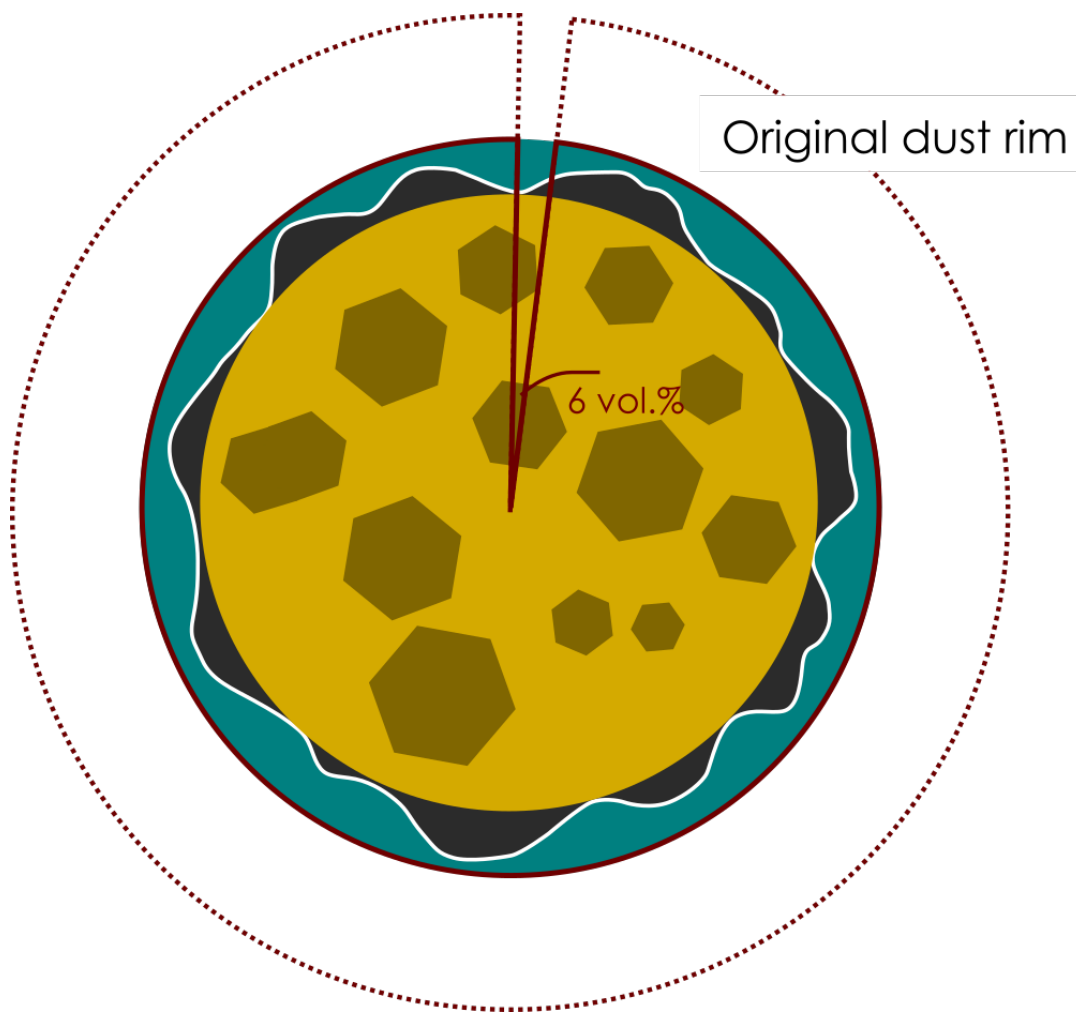
Fig. S19. Schematic of chondrule with metal rim (black) and dust rim (blue). Added in red is a slice of dust rim, which reflects the inferred volume abundance of metal in the CV dust rim using mass balance equations with data from Figure 1A in the main text.
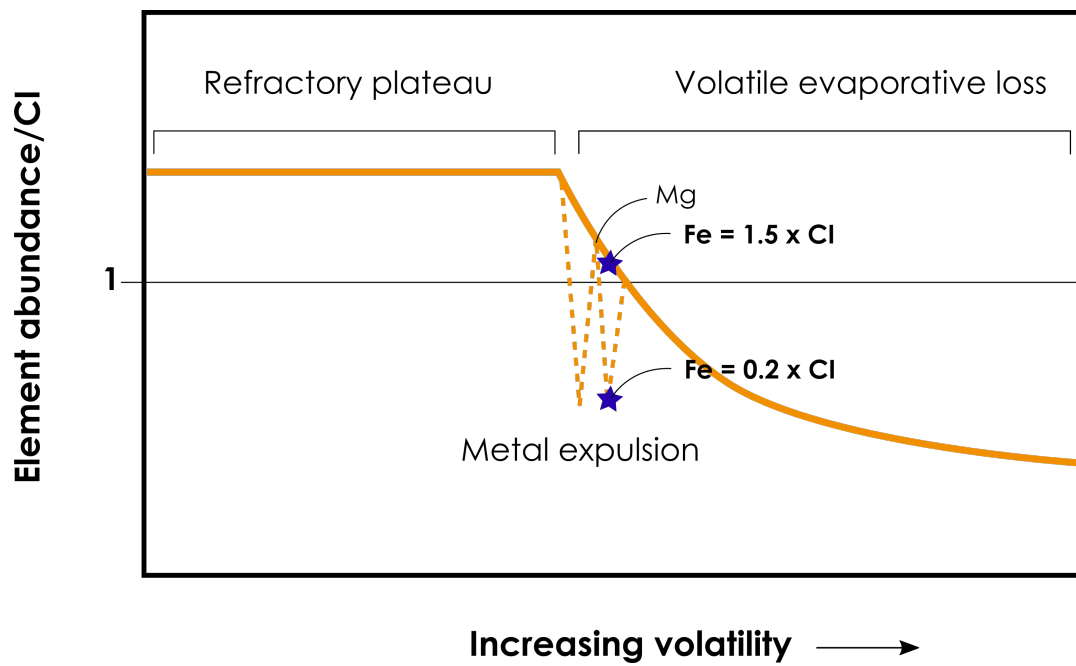
Fig. S20. Schematic of average CV chondrule volatility pattern, with a model for evaporation only (solid yellow line) and including metal expulsion during chondrule formation (dashed line).

References

1. Grossman JN, Brearley AJ (2005) The onset of metamorphism in ordinary and carbonaceous chondrites. *Meteoritics & Planetary Science* 40(1):87–122.
2. Haack H, et al. (2012) Maribo—A new CM fall from Denmark. *Meteoritics & Planetary Science* 47(1):30–50.
3. Hewins RH, et al. (2014) The Paris meteorite, the least altered CM chondrite so far. *Geochimica et Cosmochimica Acta* 124:190–222.
4. van Kooten EM, et al. (2018) Isotope record of mineralogical changes in a spectrum of aqueously altered cm chondrites. *Geochimica et Cosmochimica Acta* 237:79 – 102.
5. Schrader DL, et al. (2015) The formation and alteration of the renazzo-like carbonaceous chondrites iii: Toward understanding the genesis of ferromagnesian chondrules. *Meteoritics & Planetary Science* 50(1):15–50.
6. Wasson JT, Rubin AE (2010) Metal in CR chondrites. *Geochimica et Cosmochimica Acta* 74(7):2212–2230.
7. Briani G, et al. (2013) Short duration thermal metamorphism in CR chondrites. *Geochimica et Cosmochimica Acta* 122:267–279.
8. Harju ER, et al. (2014) Progressive aqueous alteration of cr carbonaceous chondrites. *Geochimica et Cosmochimica Acta* 139:267 – 292.
9. Rubin AE, Trigo-Rodríguez JM, Huber H, Wasson JT (2007) Progressive aqueous alteration of CM carbonaceous chondrites. *Geochimica et Cosmochimica Acta* 71(9):2361–2382.
10. Wasson JT, Rubin AE (2009) Composition of matrix in the CR chondrite LAP 02342. *Geochimica et Cosmochimica Acta* 73(5):1436–1460.
11. Newbury DE, Ritchie NWM (2015) Performing elemental microanalysis with high accuracy and high precision by scanning electron microscopy/silicon drift detector energy-dispersive X-ray spectrometry (SEM/SDD-EDS). *J Mater Sci* 50(2):493–518.
12. Jones RH, Scott ERD (1989) Petrology and thermal history of type IA chondrules in the Semarkona (LL3.0) chondrite in *Lunar and Planetary Science Conference Proceedings*, Lunar and Planetary Science Conference Proceedings, eds. Ryder G, Sharpton VL. Vol. 19, pp. 523–536.
13. Warren PH (1997) The Unequal Host-Phase Density Effect in Electron Probe Defocused Beam Analysis: an Easily Correctable Problem in *Lunar and Planetary Science Conference*, Lunar and Planetary Science Conference. Vol. 28, p. 1497.
14. Zanda B, Lewin E, Humayun M (2018) The Chondritic Assemblage in *Chondrules: Records of Protoplanetary Disk Processes*, eds. Russell S, Connolly Jr. H, Krot A. (Cambridge University Press, Cambridge), pp. 122–150.
15. Lodders K (2003) Solar System Abundances and Condensation Temperatures of the Elements. *ApJ* 591(2):1220.
16. Bland PA, Zolensky ME, Benedix GK, Sephton MA (2006) *Weathering of Chondritic Meteorites*, eds. Lauretta DS, McSween HY. pp. 853–867.
17. Braukmüller N, Wombacher F, Hezel DC, Escoube R, Münker C (2018) The chemical composition of carbonaceous chondrites: Implications for volatile element depletion, complementarity and alteration. *Geochimica et Cosmochimica Acta* 239:17–48.
18. Wlotzka F (1993) A Weathering Scale for the Ordinary Chondrites. *Meteoritics* 28.
19. Huss GR, Meshik AP, Smith JB, Hohenberg C (2003) Presolar diamond, silicon carbide, and graphite in carbonaceous chondrites: implications for thermal processing in the solar nebula. *Geochimica et Cosmochimica Acta* 67(24):4823 – 4848. A Special Issue Dedicated to Robert M Walker.
20. Clayton RN (1993) Oxygen isotopes in meteorites. *Annual Review of Earth and Planetary Sciences* 21(1):115–149.
21. Clayton RN (2003) Oxygen Isotopes in Meteorites. *Treatise on Geochemistry* 1:711.
22. Valdes MC, Moreira M, Foriel J, Moynier F (2014) The nature of Earth's building blocks as revealed by calcium isotopes. *Earth and Planetary Science Letters* 394:135–145.
23. Deng Z, et al. (2019) Titanium isotopes as a tracer for the plume or island arc affinity of felsic rocks. *Proceedings of the National Academy of Sciences* 116(4):1132–1135.
24. Qin L, Alexander CMO, Carlson RW, Horan MF, Yokoyama T (2010) Contributors to chromium isotope variation of meteorites. *Geochimica et Cosmochimica Acta* 74(3):1122 – 1145.
25. Patzer A, Hezel DC, Bendel V, Pack A (2018) Chondritic ingredients: II. Reconstructing early solar system history via refractory lithophile trace elements in individual objects of the Leoville CV3 chondrite. *Meteoritics & Planetary Science* 53(7):1391–1412.
26. Inoue M, Nakamura N, Kimura M (2009) Tetrad effects in REE abundance patterns of chondrules from CM meteorites: Implications for aqueous alteration on the CM parent asteroid. *Geochimica et Cosmochimica Acta* 73(17):5224 – 5239.
27. Mahan B, et al. (2018) Volatile element evolution of chondrules through time. *PNAS* p. 201807263.
28. DESCH SJ, MORRIS MA, CONNOLLY Jr. HC, BOSS AP (2012) The importance of experiments: Constraints on chondrule formation models. *Meteoritics & Planetary Science* 47(7):1139–1156.
29. Libourel G, Portail M (2018) Chondrules as direct thermochemical sensors of solar protoplanetary disk gas. *Science Advances* 4(7):eaar3321.
30. Bollard J, et al. (2017) Early formation of planetary building blocks inferred from Pb isotopic ages of chondrules. *Science Advances* 3(8):e1700407.
31. Olsen MB, Wielandt D, Schiller M, Van Kooten EMME, Bizzaro M (2016) Magnesium and 54Cr isotope compositions of

404 carbonaceous chondrite chondrules – Insights into early disk processes. *Geochimica et Cosmochimica Acta* 191:118–138.

405 32. Scott ER (2007) Chondrites and the protoplanetary disk. *Annual Review of Earth and Planetary Sciences* 35(1):577–620.

406 33. Hezel DC, et al. (2018) Fe isotope composition of bulk chondrules from Murchison (CM2): Constraints for parent body
407 alteration, nebula processes and chondrule-matrix complementarity. *Earth and Planetary Science Letters* 490:31–39.

408 34. Hughes DW (1980) The dependence of chondrule density on chondrule size. *Earth and Planetary Science Letters* 51(1):26 –
409 28.

410 35. Macke RJ, Consolmagno GJ, Britt DT (2011) Density, porosity, and magnetic susceptibility of carbonaceous chondrites.
411 *Meteoritics & Planetary Science* 46(12):1842–1862.

412 36. Rubin AE, Wasson JT (1987) Chondrules, matrix and coarse-grained chondrule rims in the Allende meteorite: Origin,
413 interrelationships and possible precursor components. *Geochimica et Cosmochimica Acta* 51(7):1923–1937.

414 37. Clarke RS, et al. (1971) Allende, Mexico, Meteorite Shower.

415 38. Huss GR, Alexander CMO, Palme H, Bland PA, Wasson JT (2005) Genetic Relationships between Chondrules, Fine-grained
416 Rims, and Interchondrule Matrix in *Chondrites and the Protoplanetary Disk.* Vol. 341, p. 701.

417 39. van Kooten E, Moynier F (2019) Zinc isotope analyses of singularly small samples (<5 ng Zn): investigating chondrule-
418 matrix complementarity in Leoville. *Geochimica et Cosmochimica Acta* 261:248–268.

Elishevah van Kooten, Frédéric Moynier and Arnaud Agranier